AGU PUBLICATIONS

Tectonics

RESEARCH ARTICLE
10.1002/2017TC004785

Key Points:
- We evaluate the Miocene tectonic evolution of the northwestern Andes of Colombia through a multitechnical approach
- Ongoing exhumation and deposition of middle Miocene strata with mixed provenance constrain the collision of the Panama Arc before 12 Ma
- Late Miocene exhumation of the continental margin result from subduction tectonics that followed the collisional episode

Supporting Information:
- Table S1
- Table S2
- Table S3
- Table S4
- Table S5
- Table S6
- Table S7
- Table S8
- Supporting Information S1

Correspondence to:
S. León,
sleonva@gmail.com

Citation:
León, S., Cardona, A., Parra, M., Sobel, E. R., Jaramillo, J. S., Glodny, J., … Pardo-Trujillo, A. (2018). Transition from collisional to subduction-related regimes: An example from Neogene Panama-Nazca-South America interactions. *Tectonics*, *37*, 119–139. https://doi.org/10.1002/2017TC004785

Received 26 AUG 2017
Accepted 10 DEC 2017
Accepted article online 22 DEC 2017
Published online 9 JAN 2018

Transition From Collisional to Subduction-Related Regimes: An Example From Neogene Panama-Nazca-South America Interactions

Santiago León[1], Agustín Cardona[2], Mauricio Parra[3], Edward R. Sobel[4], Juan S. Jaramillo[5], Johannes Glodny[6], Víctor A. Valencia[7], David Chew[8], Camilo Montes[9], Gustavo Posada[5], Gaspar Monsalve[10], and Andrés Pardo-Trujillo[11]

[1]Instituto de Geociências, Universidade de São Paulo, São Paulo, Brazil, [2]Departamento de Procesos y Energía, Facultad de Minas, Universidad Nacional de Colombia, Medellín, Colombia, [3]Instituto de Energia e Ambiente, Universidade de São Paulo, São Paulo, Brazil, [4]Institut für Erd- und Umweltwissenschaften, Universität Potsdam, Potsdam-Golm, Germany, [5]Departamento de Materiales y Minerales, Facultad de Minas, Universidad Nacional de Colombia, Medellín, Colombia, [6]GeoForschungsZentrum GFZ Potsdam, Potsdam, Germany, [7]School of the Environment, Washington State University, Pullman, WA, USA, [8]Department of Geology, Trinity College Dublin, Dublin, Ireland, [9]Department of Geology, Universidad del Norte, Barranquilla, Colombia, [10]Departamento de Geociencias y Medio Ambiente, Universidad Nacional de Colombia, Medellín, Colombia, [11]Instituto de Investigaciones en Estratigrafía, Universidad de Caldas, Manizales, Colombia

Abstract A geological transect across the suture separating northwestern South America from the Panama Arc helps document the provenance and thermal history of both crustal domains and the suture zone. During middle Miocene, strata were being accumulated over the suture zone between the Panama Arc and the continental margin. Integrated provenance analyses of those middle Miocene strata show the presence of mixed sources that includes material derived from the two major crustal domains: the old northwestern South American orogens and the younger Panama Arc. Coeval moderately rapid exhumation of Upper Cretaceous to Paleogene sediments forming the reference continental margin is suggested from our inverse thermal modeling. Strata within the suture zone are intruded by ~12 Ma magmatic arc-related plutons, marking the transition from a collisional orogen to a subduction-related one. Renewed late Miocene to Pliocene acceleration of the exhumation rates is the consequence of a second tectonic pulse, which is likely to be triggered by the onset of a flat-slab subduction of the Nazca plate underneath the northernmost Andes of Colombia, suggesting that late Miocene to Pliocene orogeny in the Northern Andes is controlled by at least two different tectonic mechanisms.

1. Introduction

The timing and mechanisms involved in the northern Andean orogeny may be the result of the super imposition of global plate kinematic reconfigurations, such as the westward drift of the entire South American plate (Coney & Evenchick, 2003; Russo & Silver, 1996), different subduction regimes associated with the Farallon and Nazca plates, with interspersed collision and translation of oceanic terranes (Gansser, 1973; Ramos, 1999; Spikings & Simpson, 2014). Within this complex geodynamic setting, most authors consider the collision of the Panama Arc as a the major Neogene event in the history of the margin (Amaya et al., 2017; Bermúdez et al., 2015; Farris et al., 2011; Kroonenberg et al., 1990; Montes et al., 2015). Such studies, however, document the stratigraphic and/or thermochronological record of Andean growth, away from the trench and suture zones, without discriminating whether they are subduction or collisional-related episodes.

The impact of the juxtaposition between the Panama Arc and northwestern South America on the global oceanographic and biogeographic modern configurations has been widely recognized (Bartoli et al., 2005; Burton et al., 1997; Iturralde-Vinent & MacPhee, 1999). Despite its importance, intense controversy still exists about the timing and nature of the geological processes involved. Ages as far apart as ~40 Ma and ~3 Ma have been proposed for both the early interaction and the ultimate establishment of a land connection (Bacon et al., 2015; Coates et al., 2004; Duque-Caro, 1990a; Montes et al., 2015; O'Dea et al., 2016; Pindell & Kennan, 2009). In this contribution, we integrate field observations, sedimentary provenance, U-Pb zircon geochronology, detrital apatite fission tracks, and inverse thermal modeling of multiple thermochronometers along one transect in the northwestern flank of the Western Cordillera of Colombia. It is along

this transect where the suture zone between the allochthonous Panama Arc and the South American continental margin is exposed. Our goal is to characterize the Panama and South American blocks by means of their provenance, as well as document exhumation rates and changes in the detrital record of the adjacent sedimentary basins, which are probably the consequence of the collision of these tectonic blocks and the subsequent establishment of subduction regime. The new results presented here support a middle Miocene or older collision, through a complex switch from collisional to subduction-dominated regimes.

2. Geological Framework

Since Eocene times the northwestern corner of South America has experienced major plate tectonic readjustments, including changes in plate convergence obliquity (Pardo-Casas & Molnar, 1987; Somoza & Ghidella, 2012), breaking up of the Farallon oceanic plate and formation of the Nazca and Cocos plates (Lonsdale, 2005), the collision of the Panama Arc (Duque-Caro, 1990a; Montes et al., 2015), and the onset of a flat-slab subduction regime in northern Colombia (Chiarabba et al., 2015; Ramos & Folguera, 2009; Syracuse et al., 2016; Wagner et al., 2017). Such major changes in the geodynamic configuration are recorded in the filling and exhumation history of the Upper Cretaceous-Pliocene sedimentary basins exposed along the northwestern flank of the Western Cordillera of Colombia, the Atrato Basin, and the Chucunaque-Tuira Basin in Panama (Coates et al., 2004; Duque-Caro, 1990a, 1990b) (Figure 1). The inboard stratigraphic and magmatic record of the northern Andes of Colombia has been also interpreted as the imprint of these major tectonic events (Mora et al., 2013; Parra et al., 2010; Wagner et al., 2017).

The northern segment of the Western Cordillera of Colombia is constituted by different oceanic terranes, which are tectonically juxtaposed to the continental margin as a consequence of the interaction between the Caribbean and South American plate since Late Cretaceous times (Toussaint & Restrepo, 1994; Vallejo et al., 2006; Villagómez & Spikings, 2013). The most landward and easternmost domain, located between the Uramita Fault Zone (UFZ) and the Romeral Fault System (RFS) (Figure 1), is characterized by a basaltic basement with a plateau-like geochemical signature built between 100 Ma and 88 Ma (Kerr et al., 1997, Sinton et al., 1998; Villagómez et al., 2011), on which an island arc was constructed between ~90 Ma and ~80 Ma over the leading edge of the allochthonous Caribbean Plate (Hincapié-Gómez et al., 2017; Villagómez et al., 2011; Zapata et al., 2017). This oceanic plateau-arc system, which has been interpreted as a segment of the Caribbean Large Igneous Province (CLIP) accreted during the Late Cretaceous-Paleocene (Burke, 1988; Kerr et al., 1996; Sinton et al., 1998; Weber et al., 2015), is sutured to the continental margin along the RFS (Figure 1) and is overlain by Upper Cretaceous-Paleogene hemipelagic and terrigenous sediments (Bourgois et al., 1982; Moreno-Sánchez & Pardo-Trujillo, 2003; Pardo-Trujillo et al., 2002).

West of the UFZ, the Panama Arc comprises an Upper Cretaceous-Miocene intraoceanic arc that was also built over an 89–85 Ma oceanic plateau at the trailing edge of the Caribbean plate (Bourgois et al., 1982; Buchs et al., 2010; Wegner et al., 2011). This volcanic basement is overlain by Eocene-Pliocene volcano-clastic sequences, which make up the filling of the Atrato and Chucunaque-Tuira basins (Buchs et al., 2011; Coates et al., 2004; Duque-Caro, 1990a, 1990b; Haffer, 1967), and may contain the tectono-stratigraphic record of the pre- and postcollisional history. The Uramita Fault Zone (UFZ) (Figure 1) represents the suture between the Panama Arc and the CLIP and is associated with the occurrence of highly deformed zones up to 40 km wide (e.g., Istmina Deformed Belt, IDB) (Duque-Caro, 1990a). A compilation of earthquakes between 1981 and 2016 (Figure 1b) shows a concentration of events within the Uramita fault. Nineteen out of the 26 compiled earthquakes with available focal mechanisms are within 30 km from the main trace of Uramita Fault, and they indicate a transpressional regime with stresses oriented in a NNW-SSE direction; one of the nodal planes in every earthquake has an approximate S-N strike, roughly coinciding with the strike of the Uramita Fault, and suggests that this suture zone has been reactivated.

In the northern segment of the UFZ, a series of local basins with a middle Miocene to Pliocene marine to terrestrial sediment infill overly the suture zone. These basins likely contain the erosional and exhumation record of both the Panama Arc and the South American continental paleomargin during and after their collision.

2.1. Local Geology of the Transect

The transect is located on the western flank of the Western Cordillera of Colombia, approximately 180 km northwest of the city of Medellin (Figure 1). We selected this area as it crosses the suture zone between

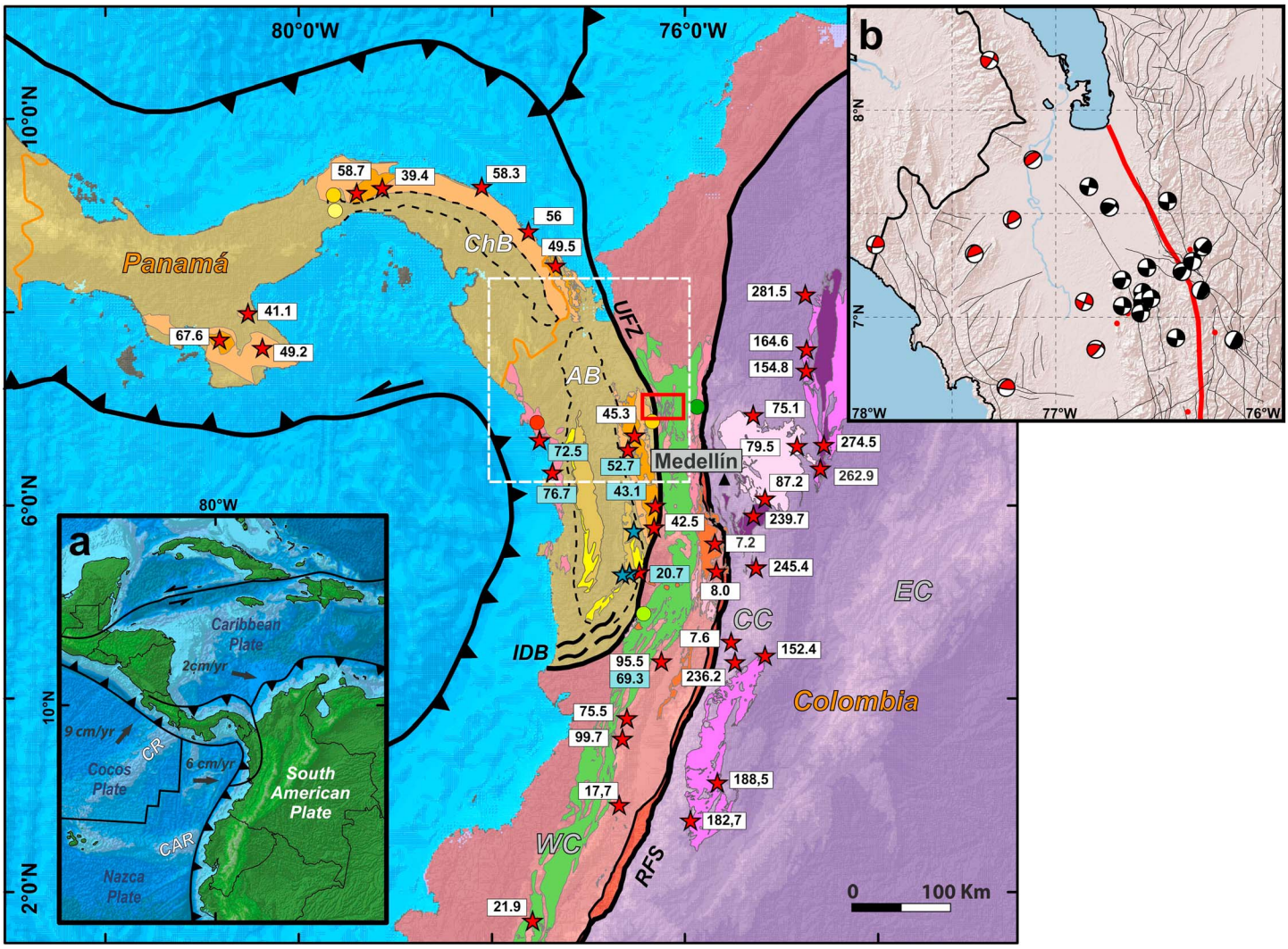

Pre-Cretaceous basement covered by Cretaceous to Neogene sediments
- Cretaceous Batholiths
- Jurassic Batholiths
- Permo-Triassic Metamorphic

Caribbean Large Igneous Province
- Island Arc-related Rocks
- Oceanic Plateau-related Rocks

Cretaceous Subduction Channel

Late Cretaceous to Paleogene Sedimentary Rocks
- Terrestrial - Hemipelagic Sediments

Panama Block
- Plutonic Rocks
- Volcanic Rocks
- Early Miocene Marine Sediments

Middle-Late Miocene Post-Collisional Transitional Continental Sediments

Middle Miocene-Pliocene Continental Arc

Fossiliferous Locality
- Early Cretaceous
- Late Cretaceous
- Eocene
- Oligocene
- Early Miocene

Others
- Geochronological Data
  - U-Pb
  - K-Ar or Ar-Ar
- Basin Border
- Study Area
- Additional Sampling Site

Figure 1. Regional tectonic and geological map modified from Gómez, Nivia, et al. (2015) showing the main morphotectonic and lithological domains of the Colombian Andes. (a) Present tectonic configuration; plate velocities are taken from Taboada et al. (2000). (b) Compilation and analysis of seismicity and focal mechanisms in the area of the Uramita Fault Zone (white rectangle in the main figure). A total of 26 mechanisms were compiled, of which 19 are within 30 km from the main trace of the Uramita Fault (black beach balls). The red alignment represents the main fault trace. Earthquakes with no available focal mechanism but with magnitude greater than 4 are shown as red dots. The focal mechanisms are consistent with NNW-SSE compression. Data were taken from the global CMT catalog (Dziewonski et al., 1981; Ekström et al., 2012), Cortés and Angelier (2005), and the catalog of the National Seismic Network of Colombia. See text for other references used. The red rectangle illustrated the location of the studied transect shown in Figure 2. Abbreviations: AB: Atrato Basin; CC: Central Cordillera; CAR: Carnegie Ridge; CR: Cocos Ridge; ChB: Chucunaque-Tuira Basin; RFS: Romeral Fault System; EC: Eastern Cordillera; IDB: Istmina Deformed Belt; UFZ: Uramita Fault Zone; WC: Western Cordillera.

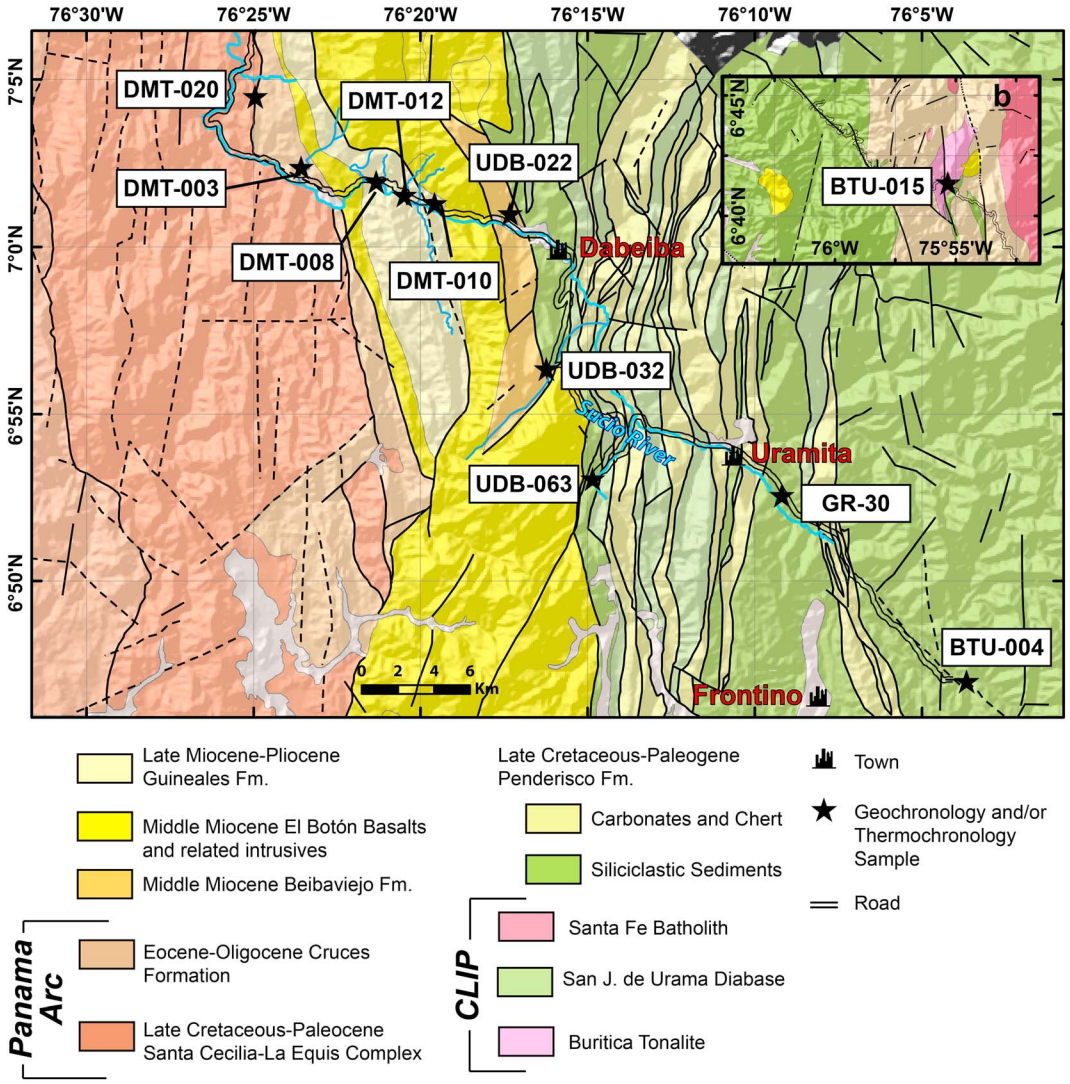

Figure 2. Local geological map of the study area after Rodríguez et al. (2013) showing the main lithological units and the location of samples use for geochronological and thermochronological analyses. (b) Location of the sample collected from the Buriticá Tonalite ~15 km farther east from the main transect shown in the map.

the Panama Arc and the South American margin. The Cenozoic continental margin is defined by the basaltic basement of the CLIP, locally known as the San Jose de Urama Diabase (Rodríguez & Arango, 2013), which also includes a 100.9 ± 0.9 Ma tonalitic intrusion known as the Buriticá Tonalite (Weber et al., 2015). The CLIP is overlain by intensely deformed turbiditic and hemipelagic sediments of Late Cretaceous-Paleogene age (Bourgois et al., 1982; Pardo-Trujillo et al., 2002), which are included within the Penderisco Formation (Álvarez, 1971) (Figure 2). The Panama Arc is represented by a volcanic basement with Ar/Ar and K/Ar ages between ~70 Ma and ~50 Ma (Bourgois et al., 1982; Buchely et al., 2009; Kerr et al., 1997) that includes porphyritic andesites and pillow lavas grouped within the Santa Cecilia-La Equis Complex (González, 2001) (Figure 2). The volcanic rocks are intruded by Eocene intermediate batholiths (e.g., Mandé and Acandí) with U-Pb zircon ages between ~60 Ma and ~40 Ma (Leal-Mejía, 2011; Montes et al., 2015). At its northern segment, the Santa Cecilia-La Equis Complex is overlain by a poorly known, highly deformed, volcanosedimentary sequence included within the Eocene-Oligocene Cruces Formation (Rodríguez et al., 2013) (Figure 2). Finally, the UFZ is covered by middle to upper Miocene hemipelagic rocks and an upper Miocene-Pliocene fluvial conglomeratic sequence, which are locally known as the Beibaviejo and Guineales formations (Rodríguez et al., 2013) (Figure 2). Both the hemipelagic and the fluvial sediments are tilted and show mostly brittle deformational features as well as shear zones. In this work we follow the

stratigraphic framework of Rodríguez et al. (2013), where the Beibaviejo Fm. is correlated with the middle level of the Beibaviejo-Amparradorcito Sediments of Mejía and Salázar (1989), for which the fossil content suggests an Oligocene-middle Miocene accumulation age. A maximum accumulation age of 9 Ma has been suggested for the Guineales Fm. based on a detrital zircon U-Pb geochronological analysis (Rodríguez et al., 2016). Farther to the west, strata of the Atrato Basin overlying the volcanic basement of the Panama Arc consist of Oligocene to early Pliocene shallowing upward sequences that pass from deep to shallow marine and transitional conditions and which have been attributed to the occurrence of tectonic disturbances during the Neogene (Duque-Caro, 1990b). In particular, the Sierra Fm., for which a middle-late Miocene accumulation age has been determined based on the large occurrence of benthic and planktic foraminifera such as specimens of *Uvigerina*, *Valvulineria*, and *Bulimina* (i.e., *Bulimina uvigerinaformis*; Duque-Caro, 1990b), is interpreted as the record of a major shallowing episode that also coincides with a stratigraphic unconformity with primary tectonic implications (Duque-Caro, 1990a, 1990b; Haffer, 1967). Equivalent strata of the Atrato Basin in Panama are preserved in the Chucunaque-Tuira Basin (Coates et al., 2004). Our sampling and field observations include the Cenozoic continental paleomargin and its basement, the allochthonous Panama Arc, and the Miocene-Pliocene sediments that are patchy covering the UFZ. Additionally, we conducted a regional sampling of the middle-upper Miocene hemipelagic sediments from the Sierra Fm., exposed toward the center and western border of the Atrato Basin (Figure 1).

3. Sampling Strategy and Methods

We described the main lithological and structural features of the rock units cropping out along the SE-NW oriented 40 km long transect, in ~100 field stations. Despite the limited exposures and intense weathering, we collected fresh samples from the Buriticá Tonalite and sandstone samples from the Penderisco, Cruces, Beibaviejo, and Guineales formations. For selected samples, we conducted petrographic, heavy mineral, geochronological, and thermochronological analyses. Our inverse thermal modeling includes apatite fission tracks and apatite and zircon U-Th/He thermochronology. We also conducted an additional sampling campaign for detrital U-Pb zircon geochronology and apatite-fission track analyses on three specific sites located farther south, where sedimentary units cover the allochthonous Panama arc (Sierra Fm.) (Figure 1). In addition, we collected a sediment sample for detrital AFT analysis from the Sucio River, which drains the western flank of the Western Cordillera and flows almost parallel to our transect (Figure 2), in order to reconstruct the modern catchment configuration and its recent integrated exhumation patterns. The analyzed sample information can be found in Table S1 in the supporting information, and the description of the methods employed is also provided in Texts S1 to S3 in the supporting information.

4. Results

Since our contribution is based on a multitechnique approach, we present the results of each analytical method followed by a brief interpretation with preliminary conclusions, which are then integrated into the overall discussion.

4.1. Lithological Features and Sedimentary Provenance

4.1.1. Field and Petrographic Observations

Three distinct lithological associations, limited by N-S oriented fault zones, were identified in our transect (Figure 2). First, the eastern Upper Cretaceous-Paleogene Penderisco Fm. (representing the South American continental margin) is unconformably overlying the CLIP basement that includes the ~100 Ma Buriticá Tonalite (Weber et al., 2015). We also sampled this tonalite as a reference for an eastern continental segment out of the suture zone. The Penderisco Formation is characterized by the occurrence of interlayered arkoses, litharenites, and siliceous mudstones with thin plane-parallel lamination and cross-bedding structures, which seemingly varies laterally from terrigenous to hemipelagic sequences to the west, represented by interlayered chert and fossiliferous biomicrites. Both, the hemipelagic and terrigenous sediments are strongly deformed by outcrop-scale folding. To the west, the UFZ constitutes the limit of an ~10 km wide high deformation zone where basaltic pillow-lavas and chert blocks are embedded within a fine-grained sheared matrix. The basaltic rocks show porphyritic and seriate textures with clinopyroxene and plagioclase phenocrysts in an altered matrix, similar to those rocks included within the San J. de Urama Diabase (Rodríguez & Arango, 2013).

Second, the central domain contains middle Miocene limestones and feldspathic litharenites and upper Miocene-Pliocene fluvial conglomerates and litharenites from the Beibaviejo and Guineales formations, respectively. Although rocks from the Beibaviejo Fm. have limited exposures within the study area, it was possible to recognize levels of massive lithic arkoses, feldspathic litharenites, and dark limestones intruded by a fine-grained plutonic rock of gabbroic composition. A suite of reddish volcanic rocks with seriate and vesicular textures defined by plagioclase and minor clinopyroxene phenocrysts in an altered hypocrystalline matrix also crop out within this central domain. Together with the intrusives, these volcanic rocks have been associated to El Botón Basalts, which are characterized by a shoshonitic geochemical signature and K/Ar and Ar/Ar ages between 12 Ma and 9 Ma (Zapata & Rodríguez, 2011). The upper Miocene-Pliocene Guineales Fm. is defined by a thick conglomeratic sequence with subordinate interlayered fine to coarse-grained litharenites, with carbonized stems and leaf prints. Bed tilting and the presence of meter-scale shear zones are common deformational features of both the Beibaviejo and Guineales formations, as well as of the volcano-plutonic rocks of the El Botón Basalts.

Finally, the western domain comprises a volcano-sedimentary association (Cruces Fm.) that includes tuffs, agglomerates, volcanic sandstones, siliceous mudstones, and limestones and which unconformably overlies a basaltic to andesitic basement. The latter includes massive and porphyritic basalts-andesites with clinopyroxene and plagioclase phenocrysts within a reddish altered matrix and minor pillow lavas defined as the Santa Cecilia-La Equis Complex. As with the eastern domain, these sequences also exhibit ductile deformation features as outcrop-scale folding and mélange structures, which were mostly recognized toward its eastern limit.

Field photographs of the lithological domains described above are presented in Figure S1 in the supporting information.

4.1.2. Sandstone Petrography and Heavy Minerals

We present in chronological order the results of sandstone petrography and heavy mineral analyses. Sandstone petrography and heavy mineral data are given in Tables S2 and S3, respectively.

The eight samples from the Upper Cretaceous-Paleogene Penderisco Fm. are fine to coarse-grained texturally immature lithic arkoses, feldspathic litharenites, litharenites, and sublitharenites (Figure 3a). Particles are subangular with low sphericity, composed of undulatory quartz, euhedral plagioclase, and lithic fragments. Rock fragments are dominantly volcanic and sedimentary with micaceous schists in minor proportion (Figure 3b). Epidote, biotite, muscovite, and pyroxene are present as accessory phases. In the tectonic discrimination diagrams most of the samples plot within the recycled orogen and continental block provenance fields, whereas in the Qp-Lv-Ls diagram, they plot close to the subduction complex and collision orogen sources (Figure 3c). Heavy minerals of the Upper Cretaceous-Paleogene Penderisco Fm. consist of a mixed suite of ultrastable (zircon, tourmaline, and rutile) and unstable and stable minerals (clinopyroxene, garnet, biotite, zoisite, apatite, muscovite, and clinozoisite) (Figure 3d).

The seven samples from the volcano-clastic Eocene-Oligocene Cruces Fm. are texturally immature fine- to coarse-grained arkoses (Figure 3a), with subangular and low-sphericity fragments, composed of euhedral plagioclase and volcanic lithic fragments. Pyroxene, amphibole, epidote, quartz, and plutonic lithics are also present in minor proportion (Figure 3b). In the tectonic discrimination diagrams the samples plot within the continental block provenance fields, whereas in the Qp-Lv-Ls discrimination diagram, they plot within and close to the arc orogen sources (Figure 3c). Sample DMT-020 from the Eocene-Oligocene Cruces Fm. is composed of stable (epidote and zoisite) and unstable minerals (clinopyroxene and orthopyroxene), with clinopyroxene as the dominant component (Figure 3d).

Two samples from the middle Miocene Beibaviejo Fm. are texturally immature, fine- to coarse-grained lithic arkoses and feldspathic litharenites (Figure 3a) with subangular and low-sphericity fragments, mostly composed of undulatory quartz and particles of sedimentary, volcanic, and metamorphic rocks (Figure 3b). In the tectonic discrimination diagrams, samples plot within the magmatic arc and recycled orogen provenance fields, whereas in the Qp-Lv-Ls diagram, samples plot within the arc orogen sources and close to the subduction complex sources, which means predominantly upper crustal sources (Figure 3c). Samples from this unit are characterized by a high content of ultrastable and stable minerals, such as zircon, rutile, tourmaline, kyanite, garnet, muscovite, and epidote-group minerals (Figure 3d).

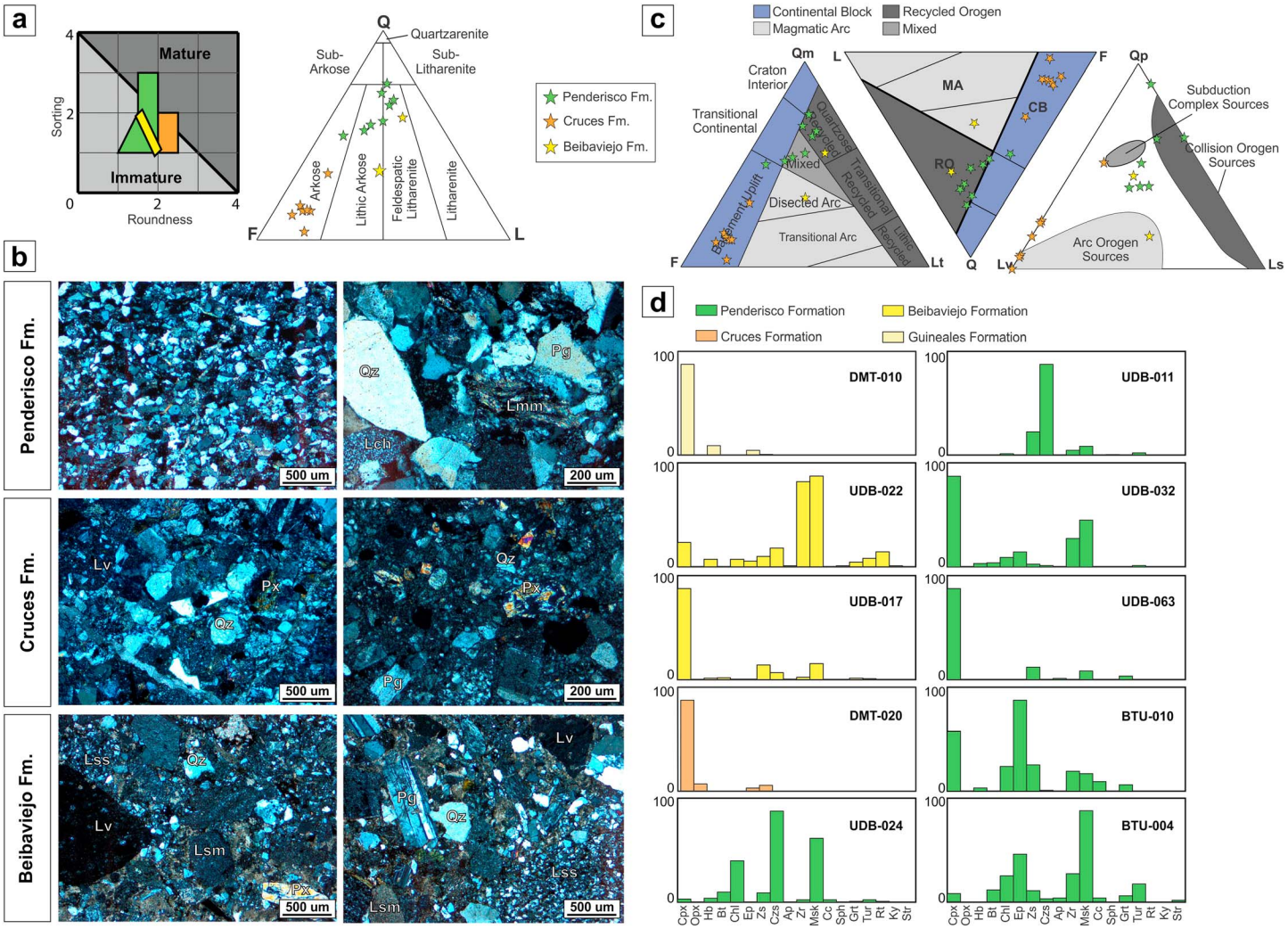

Figure 3. (a) Textural maturity assessment after Zimmermann and Hall (2016) and Q-F-L classification diagram after Folk (1980). (b) Photomicrographs of samples from the Late Cretaceous-Paleogene Penderisco Fm., Eocene-Oligocene Cruces Fm., and the middle Miocene Beibaviejo Fm. Abbreviations: Lch: Chert lithic fragment; Lmm: Micaceous metamorphic lithic fragment; Lsm: mudstone lithic fragment; Lss: sandstone lithic fragment; Lv: volcanic lithic fragment; Pg: plagioclase; Px: pyroxene; Qz: quartz. (c) Sandstone tectonic discrimination diagrams Qm-F-Lt diagram after Dickinson (1985), Q-F-L diagram after Garzanti (2016), and Qp-Lv-Ls diagram after Dickinson et al. (1983). (d) Results of the heavy-mineral analysis. Abbreviations: Ap: apatite, Bt: biotite, Cc: calcite, Chl: chlorite, Cpx: clinopyroxene, Czs: clinozoisite, Ep: epidote, Grt: garnet, Hb: hornblende, Ky: kyanite, Msk: muscovite, Opx: orthopyroxene, Rt: rutile, Sph: sphene, Str: staurolite, Tur: tourmaline, Zr: zircon, Zs: zoisite.

Sandstone beds within the Guineales Fm. have been previously described by Rodríguez et al. (2016) as wackes and litharenites, composed of lithic fragments of chert, andesite and mudstone, quartz and minor feldspar, pyroxene, hornblende, and biotite. Heavy minerals from sample DMT-010 are represented by clinopyroxene, with minor hornblende, epidote, and zoisite (Figure 3d).

4.1.3. Detrital and Magmatic Zircon U-Pb Geochronology

The zircon U-Pb geochronological data from all samples analyzed in this work are given in Table S4.

4.1.3.1. Upper Cretaceous-Paleogene Penderisco Fm.

Sample BTU-004 yielded a total of 91 detrital zircon U-Pb ages. Crystals are dominantly prismatic and euhedral with a length:width (L:W) ratio of 3:1, with subrounded grains in minor proportion. Cathodoluminescence images show oscillatory patterns related to a magmatic character, as well as minor rims surrounding oscillatory zircons that may be related to a metamorphic origin (Vavra et al., 1999). Th/U ratios range from 0.15 to 4.56, suggesting the dominance of magmatic zircons (Rubatto, 2002). Major age peaks are of Paleocene-Eocene (61–55 Ma), Late Cretaceous (92–80 Ma), Permo-Triassic (270–227 Ma), and minor Paleozoic to

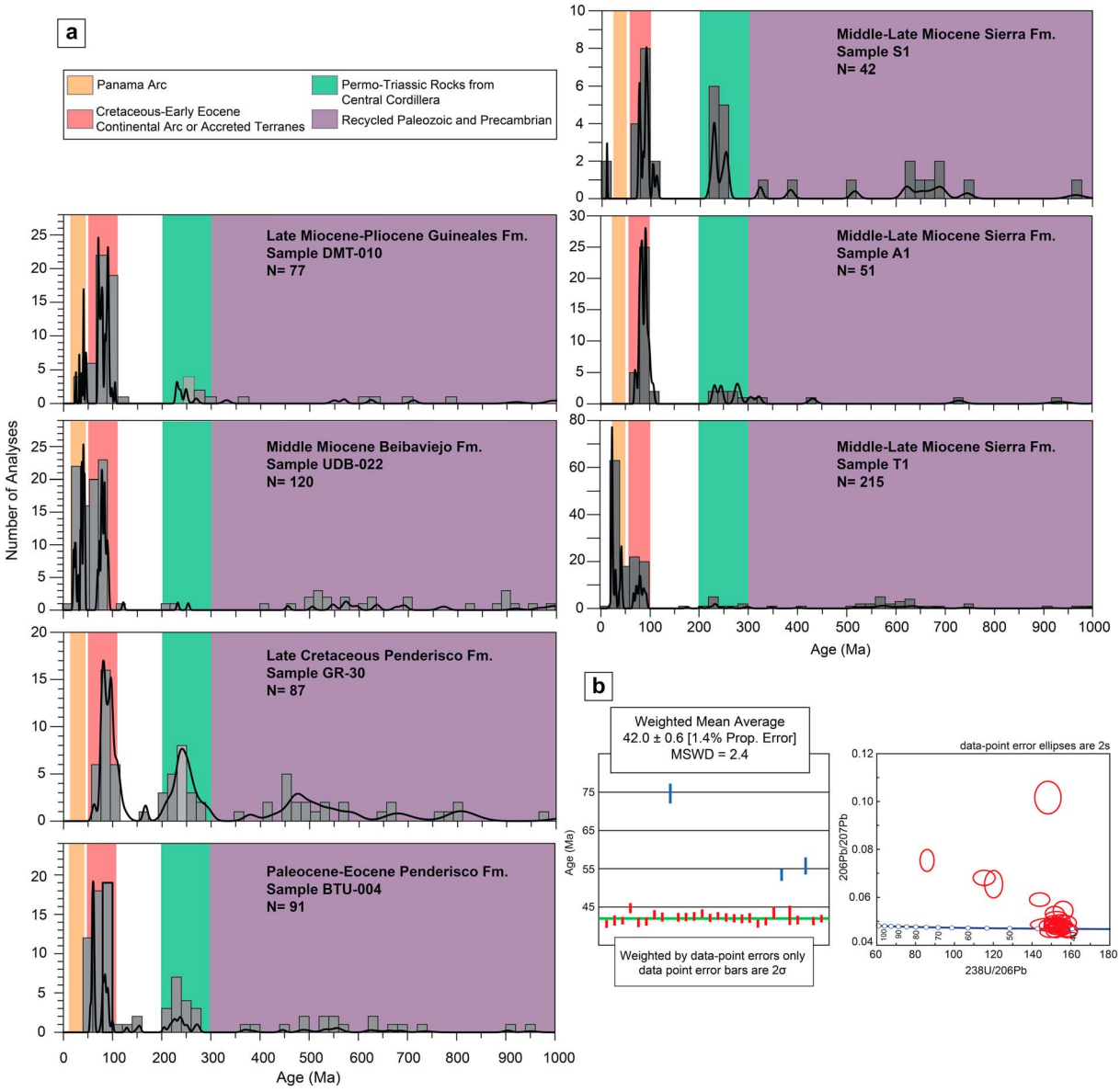

Figure 4. (a) Probability density plots (PDPs) showing the results of the detrital zircon U-Pb geochronology for samples of the Penderisco, Cruces, Beibaviejo, Guineales, and Sierra formations. (b) Weighted mean age plot and Tera-Wasserburg concordia diagram for the tuff sample DMT-003 from the Cruces Fm. Cathodoluminescence images are presented in Figure S2.

Proterozoic (~400–1,000 Ma) ages (Figure 4a). A maximum accumulation age of 55.4 ± 0.8 Ma is defined by the weighted mean of the three youngest overlapped ages (Dickinson & Gehrels, 2009).

A total of 87 individual zircon U-Pb ages were obtained from the sandstone sample GR-30 from the western segment of the Penderisco Fm. Most of the crystals are prismatic and euhedral with L:W ratio between 3:1 and 2:1. Cathodoluminescence images show oscillatory patterns characteristic of igneous rocks, with very bright patterns and resorbed rims that may also be characteristic of metamorphic rocks (Corfu et al., 2003). Th/U ratios range between 0.11 and 1.68 and indicate that most of the zircons are probably of igneous character, except by one grain with Th/U = 0.05 that yielded an age of 802.2 ± 28.1 Ma, which might indicate a metamorphic origin (Harley et al., 2007; Rubatto, 2002). Analyzed zircons yielded major age peaks of Late Cretaceous (96–80 Ma), Permo-Triassic (220–290 Ma), and less representative early Paleozoic and Proterozoic (400–1,800 Ma) ages (Figure 4a). A maximum depositional age of 76.3 ± 1.8 Ma was also established for this sample from the weighted mean of the three youngest overlapping individual ages.

4.1.3.2. Eocene-Oligocene Cruces Fm.

U-Pb zircon geochronology analyses were conducted on a tuff (sample DMT-003) collected from the Cruces Fm. Zircons are mostly prismatic with L:W ratio between 3:1 and 2:1. The cathodoluminescence images show well-developed oscillatory overgrowth characteristic of igneous rocks. Some crystals also present magmatic resorbed patterns typical of pyroclastic volcanic rocks (Corfu et al., 2003). The igneous character of the analyzed zircons is also demonstrated by the Th/U ratios, which vary between 0.39 and 2.28. A total of 25 out of 28 concordant ages yielded a weighted mean average age of 42.0 ± 0.6 Ma that is interpreted as the crystallization age (Figure 4b). This age is consistent with previously published Ar/Ar data for the so-called Dabeiba Arc (Kerr et al., 1997). Older ages of 53.4 ± 0.8 Ma, 55.7 ± 1.1 Ma, and 74.6 ± 1.3 Ma are coherent with previously published U-Pb geochronological data for the volcano-plutonic rocks of the Panama Arc (Buchs et al., 2010; Montes et al., 2015), as well as with Ar/Ar ages reported for the basalts of the Serranía de Baudó (Kerr et al., 1997), and are likely to represent inherited zircons. A probability distribution plot is also presented in Table S4. Although one sandstone sample from the Cruces Fm. (DMT-020) was also selected for detrital geochronological analysis, no zircons were recovered.

4.1.3.3. Middle Miocene Beibaviejo Fm.

A total of 120 single grain U-Pb ages were obtained from the sandstone sample UDB-022. Zircons can be divided into two groups according to its morphology. A first group is characterized by prismatic shapes with L:W ratios around 3:1 and oscillatory patterns in the cathodoluminescence images. A second group is mostly composed of prismatic and subrounded zircons with stubby and homogeneous overgrowths typical of metamorphic rocks (Corfu et al., 2003; Vavra et al., 1999). However, the Th/U ratio values ranging from 0.38 to 5.51 indicate the dominance of zircons derived from igneous sources, except by one grain with Th/U = 0.03 that yielded an age of 963.0 ± 10.2 Ma, which might indicate a metamorphic origin (Harley et al., 2007; Rubatto, 2002). Analyzed grains yield major age-peaks of Eocene-Oligocene (42–23 Ma) and Late Cretaceous (91–73 Ma) and minor Paleozoic (~570 Ma) and Proterozoic (1,362–993 Ma) (Figure 4a). The weighted mean of the three youngest overlapped analyses yielded a maximum accumulation age of 23.4 ± 0.3 Ma. This age closely overlaps with a previously published Ar/Ar age of 25.6 ± 2.6 Ma obtained from a basaltic unit that crops out nearby the location of the sample UDB-022 that is included within the so-called Chocó-Panamá Terrane (Villagómez et al., 2011), which is probably correlated with the here called Panama Arc. Furthermore, the estimated late Oligocene-early Miocene maximum accumulation age is consistent with the previously proposed biostratigraphic age for the Beibaviejo Fm. (see discussion in section 2.1).

4.1.4. Upper Miocene-Pliocene Guineales Fm.

Sample DMT-010 from the Guineales Fm. yielded a total of 77 single grain U-Pb ages. As in the sample UDB-022 from the Beibaviejo Fm., zircons can be separated into two different groups. The cathodoluminescence images show the presence of prismatic grains with L:W ratio between 3:1 and 2:1 and a characteristic oscillatory pattern of igneous rocks. Conversely, another set of zircons shows a subrounded shape with oscillatory pattern but also homogeneous overgrowths more alike with metamorphic sources. However, Th/U ratios vary from 0.19 to 4.54, evidencing the dominance of magmatic zircons (Rubatto, 2002). Analyzed zircons yielded major age peaks of middle Eocene (46–40 Ma), Late Cretaceous (90–70 Ma), Triassic (~230 Ma), and Mesoproterozoic (~1,070 Ma) (Figure 4a).

4.1.4.1. Middle Miocene Sandstones From the Atrato Basin

Three additional samples collected from the middle-upper Miocene Sierra Fm. of the Atrato Basin (sedimentary cover of the Panama Arc) were selected for zircon U-Pb detrital analyses. From sample A1 a total of 51 single grain U-Pb ages were obtained. Th/U ratios span between 0.1 and 3.8, suggesting the dominance of zircons of magmatic nature (Rubatto, 2002). Analyzed zircons have major peaks of Late Cretaceous (91–81 Ma) and Permian (278 Ma) ages, with minor Paleozoic and Proterozoic individual ages (Figure 4a). Sample S1 yielded a total of 42 single grain U-Pb ages. As in sample A1, Th/U ratios range from 0.2 to 3.7, indicating the presence of zircons dominantly magmatic in origin. Major peaks of Late Cretaceous (91–77 Ma), Permo-Triassic (253–229 Ma), and Neoproterozoic (688 Ma) ages were identified. Minor Mesoproterozoic and Paleoproterozoic individual ages are present as well (Figure 4a). Finally, sample T1 yielded a total of 215 single grain U-Pb ages. Cathodoluminescence images show that most of the crystals are prismatic and euhedral with L:W ratio of 3:1. Otherwise, analyzed zircons show two different internal patterns on the cathodoluminescence images, with the first group having an oscillatory and sector zoning patterns, characteristic of igneous rocks (Corfu et al., 2003); the second group is characterized by overgrowth rims over oscillatory patterns with several crystals showing a homogeneous fading texture; these patterns may be characteristic

of metamorphic origin zircons (Corfu et al., 2003; Vavra et al., 1999). Th/U ratios ranges between 0.1 and 7.1 indicate that zircons are dominantly of igneous origin. Individual grains have major peaks of Oligocene-Miocene (30–23 Ma), middle Eocene (41 Ma), Late Cretaceous (92–67 Ma), Triassic (232 Ma), Neoproterozoic (1,000–570 Ma), and Paleoproterozoic-Mesoproterozoic (2,000–1,200 Ma) ages (Figure 4a).

4.1.4.2. Provenance Interpretation

The Penderisco Fm. rests nonconformably over the oceanic terranes forming the CLIP. This unit includes sandstone with unstable framework material, such as plagioclase, epidote, biotite, clinopyroxene, and volcanic lithic fragments, which indicate that these sediments were rapidly accumulated in the proximity to the source terranes. The coexistence of siliciclastic rocks with chert and fossiliferous limestones suggests accumulation in a transitional to marine environment. The quartz-rich composition and the presence of micaceous metamorphic lithic fragments, together with a mixed suite of heavy minerals such as clinopyroxene, epidote, clinozoisite, kyanite, rutile, garnet, and tourmaline, suggest that medium to high-grade metamorphic and intermediate-acid plutonic rocks, as well as basic volcanic units, were the main sources for these sediments. The U-Pb detrital signature of sandstones from this unit (samples GR-30 and BTU-004) is characterized by Cretaceous and Permo-Triassic populations, which resemble the crystallization ages from (1) either intermediate, acid plutonic rocks exposed along the axis of the Central Cordillera (e.g., Antioqueño Batholith and Quebradagrande Complex) (J. S. Jaramillo et al., 2017; Leal-Mejía, 2011; Villagómez et al., 2011) or basic, intermediate intrusives rocks from the Western Cordillera (e.g., Buriticá Tonalite, Buga Batholith, Altamira Gabbro, Santa Fe, and Sabanalarga Batholiths) (Villagómez et al., 2011; Weber et al., 2015; Zapata et al., 2017) and (2) the pre-Cretaceous metamorphic and igneous basement units of the Central Cordillera (Martens et al., 2014; Restrepo et al., 2011; Vinasco et al., 2006). Minor Paleozoic and older ages are likely to be the result of recycled material from the meta-sedimentary units that crop out along the Central Cordillera (e.g., Cajamarca Complex) (Cochrane et al., 2014; Martens et al., 2012). Late Cretaceous-early Paleocene accumulation ages have been suggested for the Penderisco Fm. (Bourgois et al., 1982; González, 2001; Pardo-Trujillo et al., 2002) based on its fossiliferous content. We interpret the Penderisco Fm. as a syn to postcollisional sequence of a Late Cretaceous-Paleocene tectonic event related to the accretion of the leading edge of the CLIP, recording the late stages of the construction of the Cenozoic continental margin of northwestern South America. Coeval widespread tectonic instability has been documented in the northern Colombian Andes, as suggested by (1) moderately rapid exhumation of the Central Cordillera between 70 and 75 Ma (Villagómez & Spikings, 2013), (2) changes on the geochemical signature from tholeiitic to high-K calc-alkaline of Cretaceous magmatic rocks exposed on the western flank of the Central Cordillera at ca. 70 Ma (J. S. Jaramillo et al., 2017), and (3) shallowing of sedimentary facies and deformation in the Colombian foreland basins (Bayona et al., 2013; Cooper et al., 1995; Gómez et al., 2003; Mora et al., 2013).

The Cruces Formation, in the Panama Arc domain, contains sandstones with a high content of euhedral plagioclase, clinopyroxene, and volcanic lithic fragments, as well as heavy minerals characteristic of basic to intermediate igneous sources, and compositional characteristics similar to those resulting from the erosional trends of magmatic arcs. All these elements and the U/Pb zircon age of 42.0 ± 0.6 Ma in a tuff suggest that this unit is part of the Eocene-Oligocene subaerial volcanism and continuous denudation of the Panama Arc. Subduction initiation and thus the magmatic activity related to the construction of the Panama Arc occurred ca. 70 Ma on the trailing edge of the CLIP. This has been interpreted as a direct consequence of the tectonic plate readjustments that followed the collision of the leading edge of the CLIP with northwestern South America (Buchs et al., 2010; Wegner et al., 2011). By middle Eocene times, this island arc was being constructed at a well-established subduction zone in which pyroclastic activity and subaerial exposure have been already documented in the Panama area (Montes, Cardona, et al., 2012; Ramírez et al., 2016).

The Oligocene-middle Miocene Beibaviejo Fm. seems to overlie the Panama Arc and the South American margin and therefore provides a minimum date for the approach and juxtaposition of both domains. It consists of hemipelagic texturally immature sediments with a mixed compositional character, including both unstable and ultrastable framework materials, such as epidote, clinopyroxene, volcanic lithics, zircon, tourmaline, rutile, and quartz. The sedimentary recycling is also evidenced by the presence of sandstone and mudstone fragments. The above suggests that the source for this unit consisted of a mixture of volcanic and uplifted sedimentary terrains in proximal shallow marine environments. Results from the U-Pb detrital geochronology of the sample UDB-022 suggest the dominance of Oligocene to middle Eocene, Late Cretaceous, and Proterozoic sources. As suggested by the petrographic and heavy mineral analyses

indicating high content of ultrastable material and sedimentary lithics, the Penderisco Fm. must have contributed detritus to this middle Miocene unit, and thus, the Cretaceous and older U-Pb detrital ages probably represent a recycling signal of the lithological domains mentioned above. The most outstanding aspect is the appearance of middle Eocene to Oligocene detrital U-Pb ages (41–30 Ma), which are arguably derived from the Panama Arc (Montes et al., 2015), since no similar ages have been reported so far for crystalline massifs included within other lithological domains or terrains in the Colombian Andes (Gómez, Montes, et al., 2015; C. Jaramillo et al., 2017). As mentioned in section 4.1.3.3, the presence of an age population around 23 Ma in the sample UDB-022 from the Beibaviejo Fm., which closely overlaps with the previously published Ar/Ar age of ca. 25 Ma for the Dabeiba Fm. included within the Chocó-Panamá Terrane (Villagómez et al., 2011), also supports our interpretation that the Panama Arc sourced this sedimentary unit.

Heavy minerals of the upper Miocene-Pliocene Guineales Fm. are dominantly represented by clinopyroxene, suggesting the dominance of basic-intermediate igneous sources. Previous geochemical and geochronological data (Rodríguez et al., 2016) indicate a rather mixed provenance including massive volcanic and porphyritic sources, as well as reworked sedimentary units. Their geochemical data show the presence of volcanic clasts with a shoshonitic signature similar to that described for rocks from the El Botón Basalts and related middle Miocene intrusives (Rodríguez & Zapata, 2012; Zapata & Rodríguez, 2011). This was used to propose a maximum accumulation age of 9 Ma for the Guineales Fm. The detrital U-Pb signature of the sample DMT-010 from the Guineales Fm. resembles that of the Penderisco Fm., with major peaks in Late Cretaceous, Permo-Triassic, and Mesoproterozoic ages, indicating a recycled U-Pb signal. However, the presence of an age population of middle Eocene (46–40 Ma), as in the Beibaviejo Fm., suggests that the Panama Arc could also provide detritus for this upper Miocene-Pliocene conglomeratic sequence.

4.2. Low-Temperature Thermochronology (ZHe, AFT, and AHe) and Inverse Thermal Modeling

In this section, we present the results of our multitermochronometer analysis and the inverse thermal modeling. Exhumation rates are estimated by using a geothermal gradient between 20°C/km and 15°C/km, which have been suggested as average values for subduction-related settings (Dumitru, 1991; Henry & Pollack, 1988). Since all samples selected for thermochronological analyses were collected far from younger intrusive units, we interpret that cooling signals are related to erosional exhumation rather than thermal relaxation after local igneous activity. The thermochronological data from all samples analyzed here (including AFT, AHe, and ZHe) are given in Tables S5 to S7.

4.2.1. Buriticá Tonalite

We selected sample BTU-015, recovered from the Buriticá Tonalite (U-Pb zircon age of 100.9 ± 0.9 Ma, Weber et al., 2015), for ZHe and AHe analyses. Three zircons yielded reproducible individual ZHe ages with a weighted mean of 52.7 ± 1.1 Ma. Four analyzed apatites yielded reproducible AHe ages with a weighted mean of 6.7 ± 0.6 Ma. An individual AHe age of 3.9 ± 8.4 Ma was discarded because of its high analytical error (over 100%).

4.2.1.1. Thermal History: Exhumation of the CLIP Basement

It seems likely that the Buriticá Tonalite was a possible source for the detritus of the Penderisco Formation (see above the results of the detrital zircon U-Pb analysis of samples GR-30 and BTU-004), given the presence of several individual ages around 100 Ma (Figure 4a). It is therefore likely that this tonalitic body (sample BTU-015) was near the surface at the time of accumulation of the Penderisco Fm. Under this assumption, good models show that the onset of cooling is not well constrained by the data; however, the thermal model that best fits the ZHe and AHe ages obtained from the Buriticá Tonalite shows that the onset of cooling/exhumation probably occurred around 50 Ma at slow rates around 0.2 km/Myr, which slightly decreased to 0.15 km/myat ca. 33 Ma and remained constant until ~4 Ma. Thereafter, a pulse of rapid exhumation with rates up to 0.6 km/Myr is registered from the early Pliocene to present (Figure 5).

4.2.2. Upper Cretaceous–Paleogene Penderisco Fm.

Five zircon grains from sandstone sample UDB-032 yielded individual ZHe ages ranging from 114 Ma to 29 Ma. This sample also yielded an AFT age of 13.1 ± 1.6 Ma, $P(\chi^2)$ = 39.3%. Only one apatite grain was successfully dated for AHe and yielded an age of 3.3 ± 0.5 Ma, with other three measured aliquots being nonapatites with no helium present. Similarly, five analyzed grains from the sample UDB-063 yielded individual ZHe ages that vary between 123 Ma and 30 Ma. For this sample, an AFT age of 14.2 ± 2.2 Ma,

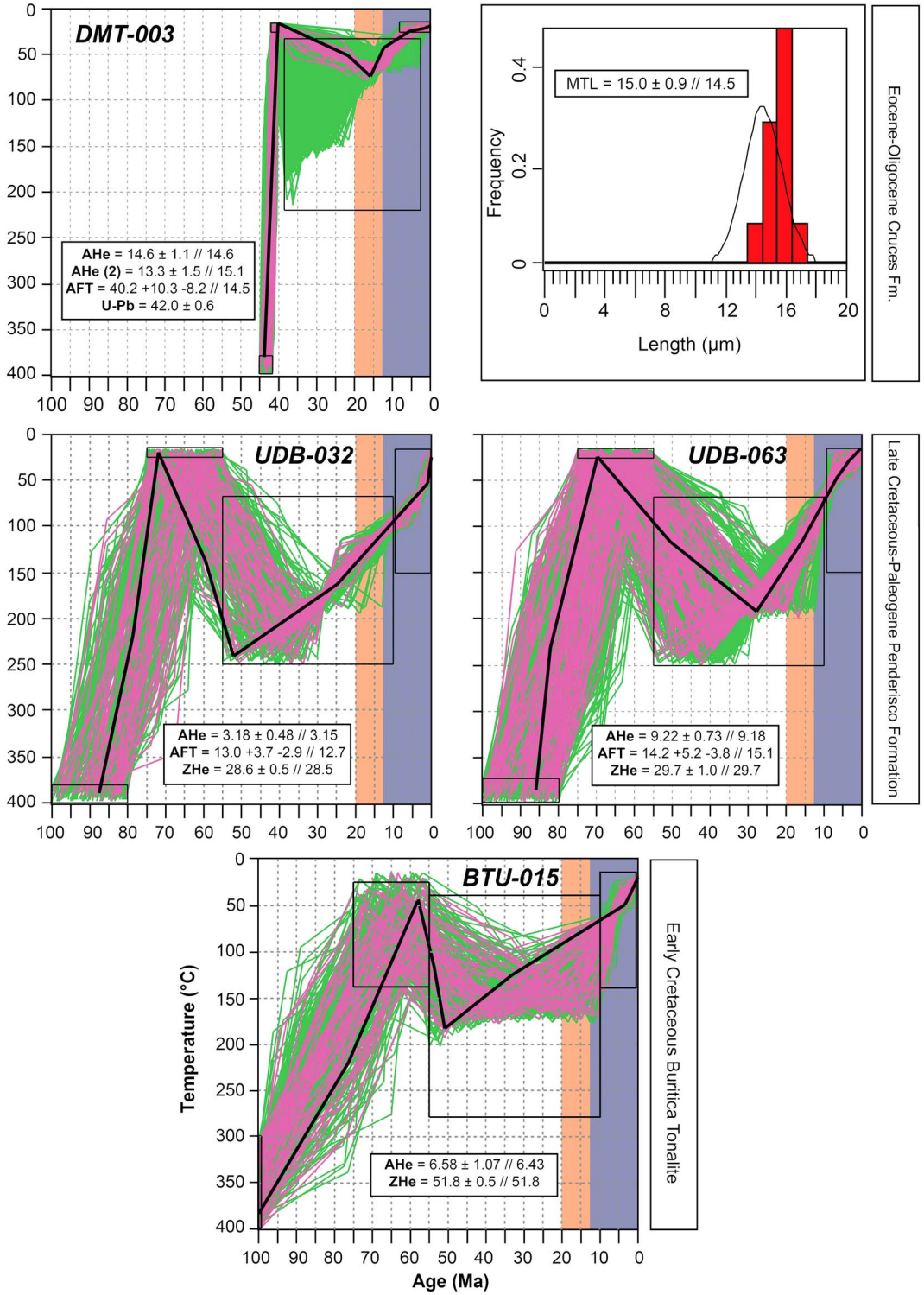

Figure 5. Inverse thermal models of the Buriticá Tonalite and the Penderisco and Cruces Fms. The boxes show the measured and modeled age for each thermochronometer obtained from the HeFTy software.

$P(\chi^2)$ = 81.2%, was obtained. Additionally, five individual reproducible AHe ages yielded a weighted mean age of 8.9 ± 0.3 Ma.

4.2.2.1. Thermal History of the Penderisco Fm.

The youngest ZHe individual ages of 29.0 ± 0.6 Ma and 49.2 ± 1.1 Ma, obtained from the sample UDB-032 from the Penderisco Fm., exhibit the highest values of effective uranium (*e*[*U*]: 870.6 ppm and 640.2 ppm, respectively) showing a negative *e*[*U*] versus age correlation pointing for a potential radiation damage effect (see Figure S3). Older ZHe ages (>66.8 Ma) show similar *e*[*U*] values (~330 ppm) and are here interpreted as detrital nonreset ages, since the lower *e*[*U*] and thus the absence of radiation damage prevented the He to be easily diffused from the zircon grains (Guenthner et al., 2013; Johnson et al., 2017). After modeling with all individual ages younger than the maximum depositional age (~55 Ma), which could represent partially or totally reset cooling ages, no good models (GOF > 0.5; Ketcham, 2005) were obtained. Therefore, we use only the youngest ZHe age of 29.0 ± 0.6 Ma, since its highest *e*[*U*] concentration suggests that this grain potentially suffered enough radiation damage to facilitate the He diffusion reducing its closure temperature and consequently yielded a reset age (Guenthner et al., 2013). Under this assumption, this ZHe age represents an approximate age for the onset of cooling. Conversely, younger ZHe ages of 35.7 ± 0.5 Ma and 30.1 ± 1.0 Ma from sample UDB-063 show the lowest values of *e*[*U*] (318.1 ppm and 67.1 ppm, respectively; see supporting Figure S3). Older ZHe ages have higher *e*[*U*] values with a slightly defined negative correlation with age, suggesting an incipient progressive radiation damage effect (progressive decrease in the closure temperature), more evidenced in the 50 Ma age that is likely to be a partially reset detrital signal. After modeling with all individual ages younger than the maximum accumulation age (~55 Ma), which could represent partially or totally reset cooling ages, no good models were obtained. Therefore, we interpret that the youngest age of 30.1 ± 1.0 Ma (with the lowest value of *e*[*U*] = 67.1 ppm) did not experience enough radiation damage to trap He atoms and is more likely to represent a reset age since the temperature required to diffuse He from this crystal was probably lower than that needed in the other four aliquots (Guenthner et al., 2013; Johnson et al., 2017).

The thermal modeling paths that best reproduce the input data for sample UDB-032 suggest that the onset of cooling/exhumation occurred between ~50 Ma and 35 Ma when the sample began to exhume at rates of approximately 0.2–0.1 km/Myr (Figure 5). The maximum temperature reached by this sample is seemingly imposed by the constraint box. However, we suggest that sample UBD-032 did not exceed ~250°C based on the textural and microtextural observations and because of the presence of nonreset individual ZHe ages older than the maximum accumulation age. Most of the good paths show a slight increase of the exhumation rates at ca. 23 Ma to ~0.3 km/Myr, which remained constant until between ~3 Ma and 1 Ma, when rates sharply increased to 1.0–0.7 km/Myr (Figure 5). Sample UDB-063 was continuously buried until anytime between ~50 and 20 Ma when it started exhuming at moderately rapid rates of ~0.4 km/Myr (Figure 5). At ca. 15 Ma a pulse of moderately rapid exhumation is registered with slightly increased rates between 0.5 km/Myr and 0.4 km/Myr, which remained until present (Figure 5).

4.2.3. Eocene–Oligocene Cruces Fm.

Sample DMT-003, with a zircon U-Pb crystallization age of 42.0 ± 0.6 Ma, yielded three reproducible individual ZHe ages with a weighted mean of 44.7 ± 0.4 Ma. Apatite fission track analysis yielded an age of 40.2 ± 4.6 Ma, $P(\chi^2)$ = 100%, and a mean track length of 15.0 ± 0.9 μm, despite the limited amount of horizontal confined tracks found (up to 10). AHe analyses conducted on this sample yielded individual ages spanning from 38 Ma to 13 Ma.

4.2.3.1. Thermal History of the Cruces Formation

Conflicting U-Pb and ZHe ages in sample DMT-003 from the tuff sample of the Cruces Fm. may be the consequence either of an overcorrection of the ZHe age by the geometric factor (Farley et al., 1996) or the presence of microinclusions that tend to produce an excess of U and yield older ages (Fitzgerald, 2006). ZHe ages obtained for this sample are therefore not considered for thermal modeling. On the other hand, AFT and AHe analyses conducted in this sample show that younger AHe ages of 13.1 ± 0.7 Ma and 14.2 ± 0.5 Ma are partially reset ages, since the presence of long fission tracks (~15 μm) (Figure 5) suggests that this sample did not achieve temperatures above the apatite partial annealing zone (~60–120°C, Reiners & Brandon, 2006).

The robust models obtained from the inverse thermal modeling of sample DMT-003 from the Cruces Fm. suggest that after its formation, the sample was buried until ca. 14 Ma, reaching maximum temperatures within the apatite-helium partial retention zone (Figure 5). At this moment, it started to be exhumed at rates

between 0.8 km/Myr and 1.0 km/Myr. Following the period of rapid exhumation, rates started to progressively decrease until present.

4.2.4. Upper Miocene-Pliocene Guineales Fm. and Modern Sediments From the Sucio River

Apatite fission track analyses were conducted in two samples from the Guineales Fm. Due to a moderate apatite yield, only a total of 41 grains were analyzed from the sample DMT-010. With a $P(\chi^2) = 0\%$, individual ages are mostly grouped around ~12–24 Ma, ~40 Ma, and ~70 Ma, with less representative older ages (>100 Ma) (Figure 6). A maximum accumulation age of 5.5 ± 2.6 Ma was estimated from the detrital AFT ages and is defined by the weighted mean age of the three youngest overlapped individual grains. Apatite (U-Th/He) analyses were also conducted on four aliquots from this sample. Individual ages of 4.9 ± 0.6 Ma, 5.2 ± 1.7 Ma, 6.5 ± 1.0 Ma, and 13.9 ± 1.0 Ma were obtained.

Sample DMT-008 from the Guineales Fm. was also selected for AFT analyses. A total of 44 grains yielded an age distribution that closely resembles that obtained for sample DMT-010, with most of the ages clustered at ~12–22 Ma, ~40 Ma, and ~68 Ma (Figure 6). Although this sample passed the chi-square test ($P(\chi^2) = 57.9\%$), we interpret these ages as a detrital, nonreset cooling ages given its lithological similarities and proximity with the sample DMT-010 (~3 km, Figure 2). A maximum accumulation age of 10.6 ± 5.5 Ma was estimated from the detrital AFT ages and is defined by the weighted mean age of the three youngest overlapped individual grains.

Additionally, AFT analyses were conducted on a sample collected from the active sediments in the Sucio River. This sample serves to outline the modern cooling rates of units exposed nearby. The distribution of the individual ages resembles those observed for samples DMT-010 and DMT-008 from the Guineales Fm, with most of the individual ages grouped at ~10–15 Ma, ~40 Ma, and ~60 Ma (Figure 6). However, the proportion of ages clustered at ~40 Ma became more representative. The weighted mean of the three youngest overlapped individual grains yielded a maximum accumulation age of 4.5 ± 0.9 Ma.

4.2.4.1. Significance of the Detrital AFT and AHe Ages of the Guineales Fm. and Modern Sediments

The detrital nonreset character of the obtained AFT ages the Guineales Fm. is supported by as follows: (1) individual ages are mostly older than the maximum depositional age of 9 Ma previously suggested (Rodríguez et al., 2016) and (2) because individual ages closely resemble the AFT ages yielded by the Penderisco and Cruces Fm., which are potential sources for this sedimentary unit as discussed above in the sedimentary provenance section. Although this reasoning is more complicated when exploring the significance of the AHe individual due to the limited amount of analyzed grains, we interpret that this unit shows nonreset detrital AHe ages from the nearby sources because (1) the AHe dispersion observed in sample DMT-010 cannot be explained by $e[U]$ and grain size and (2) like the AFT analysis, individual AHe ages resemble those cooling ages obtained for samples UDB-063 from the Penderisco Fm (~5–9 Ma) and DMT-003 from the Cruces Fm. (~14 Ma). In this scenario, the youngest AHe age of 4.9 ± 0.6 Ma, which closely overlaps with the youngest AFT age population of 5.5 ± 2.6 Ma, is likely to represent the maximum accumulation age for the Guineales Fm., which is coherent with the previously suggested age < 9 Ma (Rodríguez et al., 2016). Nevertheless, further biostratigrpahic analysis and/or a larger amount of thermochronological ages will surely constrain more precisely the depositional age for the Guineales Fm.

On the other hand, the youngest AFT age population obtained in the modern sediments of the Sucio River (sample DMT-012) yielded a peak of 4.7 ± 1.0 Ma, which is equivalent to the lag time (Ruiz et al., 2004), since the depositional age for this sample is 0 Ma. Therefore, by assuming an average closure temperature of 110°C for the AFT system (Reiners & Brandon, 2006), a constant geothermal gradient between 20°C and 15°C, a surface temperature of ~20°C, and a steady state cooling (Brewer et al., 2003; Garver et al., 1999), we can estimate integrated exhumation rates between 0.8 km/Myr and 1.6 km/Myr since the late Miocene-early Pliocene in the catchment area.

4.2.5. Middle Miocene Sediments From the Atrato Basin

Sample T1 from the Sierra Fm. was also analyzed by AFT. Due to the limited apatite yield, only a total of 28 individual ages were obtained, which mainly cluster at ~13 Ma and ~32–40 Ma, with minor peaks between ~60–80 Ma and 100 Ma and older (Figure 6). A maximum accumulation age of 13.0 ± 6.0 Ma was estimated from the weighted mean age of the three youngest overlapped individual grains.

Although this sample passed the chi-square test ($P(\chi^2) = 24\%$), we interpret these ages as a detrital cooling signal, since no field evidence indicating that this unit reached temperatures above ~70°C were observed

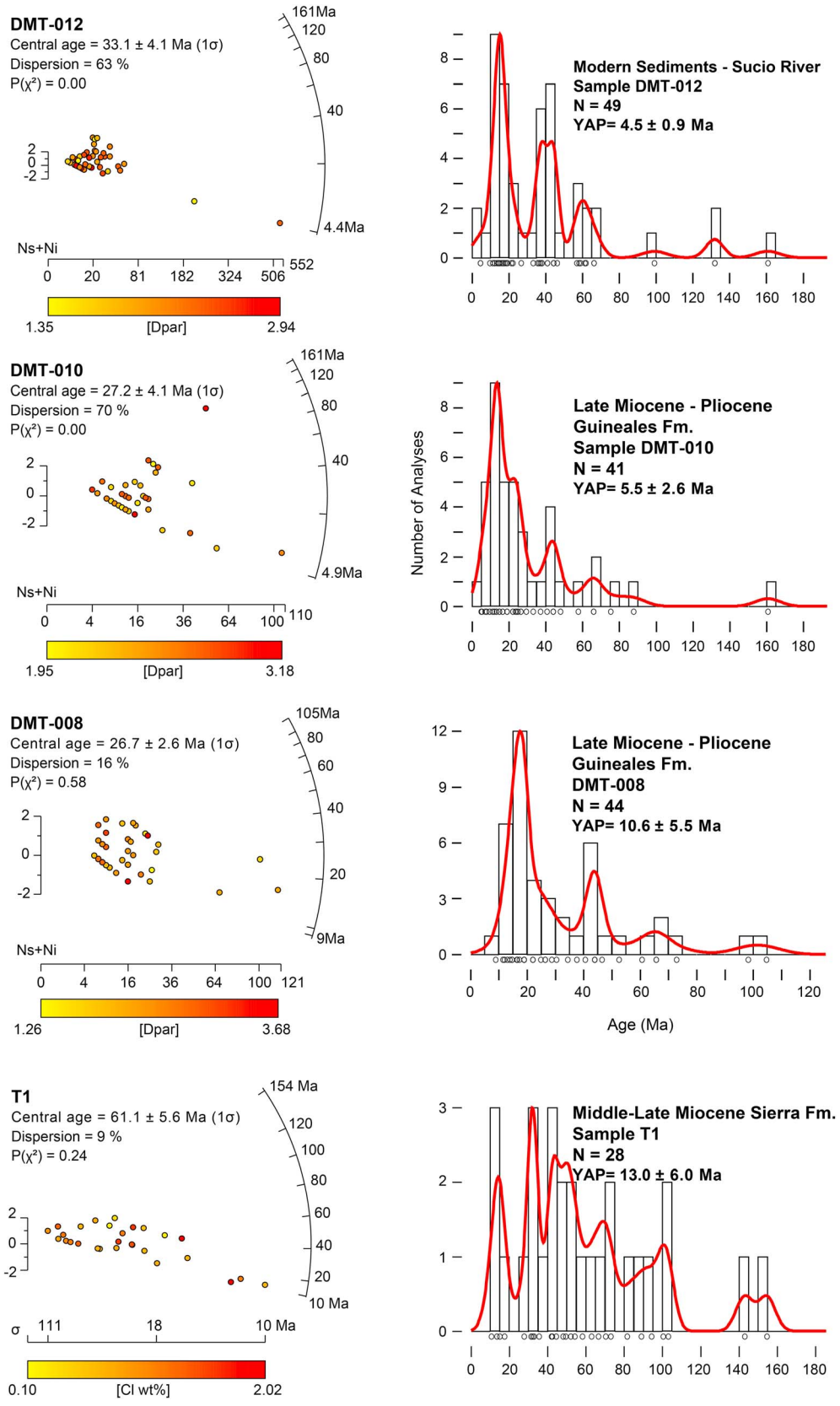

Figure 6. Radial and kernel density estimator (KDE) plots (Vermeesch, 2009, 2012) showing the results of the detrital AFT analysis of samples from the Guineales and Sierra Fms., as well as the modern sediments from the Sucio River. YAP: Youngest age population.

and because similar AFT cooling ages have been reported for the potential source domains suggested from the sedimentary provenance analysis, as the Penderisco Fm. (AFT ages around 13–14 Ma), the Panama Arc (AFT ages around 40 Ma) (Montes, Cardona, et al., 2012; Ramírez et al., 2016). The above corroborates that the middle to late Miocene sediments of the Atrato Basin, which overly the Panama Arc, were sourced by both the South American-related and the allochthonous Panamanian terranes.

5. Discussion

The new results, together with previously published geochronological and stratigraphic data, allow us to corroborate that docking of the Panama Arc predate ~12 Ma, and to better discriminate periods of increased tectonic activity during the Neogene.

The Penderisco Fm. was initially accumulated in proximal marine and transitional environments over the leading edge of the CLIP after its accretion to the northwestern corner of South America during Late Cretaceous times (~75–65 Ma) (Vallejo et al., 2006; Villagómez & Spikings, 2013). Our new geochronological data also suggest that the Penderisco Fm. records a long sedimentation history since the Late Cretaceous at least until early Eocene times, as suggested by the ca. 55 Ma detrital zircon population. Plate tectonic reorganization around the time of accumulation of the Penderisco Formation includes the subduction initiation at the trailing edge of the CLIP, the formation of the intraoceanic Panama Arc (Buchs et al., 2010), and the switch from a N to ENE displacement of the Farallon Plate between ~50 Ma and ~30 Ma (Pardo-Casas & Molnar, 1987; Somoza & Ghidella, 2012). These events, together with the fragmentation of the Farallon Plate at ca. 23 Ma (Lonsdale, 2005), may be recorded in the thermal history of this unit, with an onset of cooling/exhumation between ~50 Ma and 20 Ma. Contemporary exhumation and orogenic propagation inboard the continent have also been recorded in the Colombian and Ecuadorian Andes (Caballero et al., 2013; Parra, Mora, Jaramillo, et al., 2009; Parra, Mora, Sobel, et al., 2009; Parra et al., 2012; Saylor et al., 2012; Spikings et al., 2010; Villagómez & Spikings, 2013).

The provenance analysis of the Oligocene-middle Miocene Beibaviejo Fm. shows a mixed composition that includes detritus derived from the South American continental terranes and the Panama Arc. Strata of the Oligocene-middle Miocene Beibaviejo Fm. are patchy overlying the suture zone and intruded by 9–12 Ma mafic and intermediate plutonic rocks from El Botón basalt unit (Zapata & Rodríguez, 2011). These cross-cutting relationships, along with the mixed provenance (both Panama Arc and South American sources), constrain the docking of the Panama Arc to be pre-12 Ma (Figure 7). As previously suggested in Montes et al. (2015), our geochronological and thermochronological data confirm the presence of Panama-related sources in immature strata of middle Miocene age or younger, along the suture zone (Beibaviejo Fm.). The middle-upper Miocene Sierra Fm also shows a mixed provenance. This unit, however, unambiguously rests on Panama Arc basement (in the Atrato Basin), providing strong evidence that by middle Miocene times, the South American margin was providing detrital material to the Panama Arc. At that time, between 20 and 10 Ma, the Penderisco Fm. was being moderate to rapidly exhumed (~0.4 km/Myr) as a consequence of the tectonic instability triggered by the collisional episode.

Increased tectonic instability during middle Miocene times has been also documented throughout the northwestern Andes and southern Central America from the analysis of the magmatic and deformational record of the region and has been attributed to the collision of the Panama Arc with northwestern South America (Farris et al., 2017, 2011; Montes, Bayona, et al., 2012; Ramírez et al., 2016; Villagómez & Spikings, 2013) (Farris et al., 2017, 2011; Montes, Bayona, et al., 2012; Ramírez et al., 2016; Spikings et al., 2010; Villagómez & Spikings, 2013). Exhumation, increased accumulation rates, and switch from mudstone facies to fluvial conglomeratic facies also document increased instability inboard the continent, in the inter-Andean Magdalena Valley and Eastern Cordillera (Reyes-Harker et al., 2015, and references therein). Such framework is consistent with the timing of exhumation and provenance patterns documented here for the Miocene sediments in the suture zone and the Atrato Basin. Coeval environmental changes are also registered in the stratigraphic record of both the Atrato and Chucunaque-Tuira basins, where a substantial shallowing episode marked the transition from lower to upper bathyal depths during the accumulation of the Sierra Fm. that followed a major regional unconformity around 12 Ma (Coates et al., 2004; Duque-Caro, 1990b).

Recently, Wagner et al. (2017) used the spatiotemporal distribution of magmatic rocks to test models of the establishment of a shallow slab geometry in the Colombian Andes, particularly the formation of a

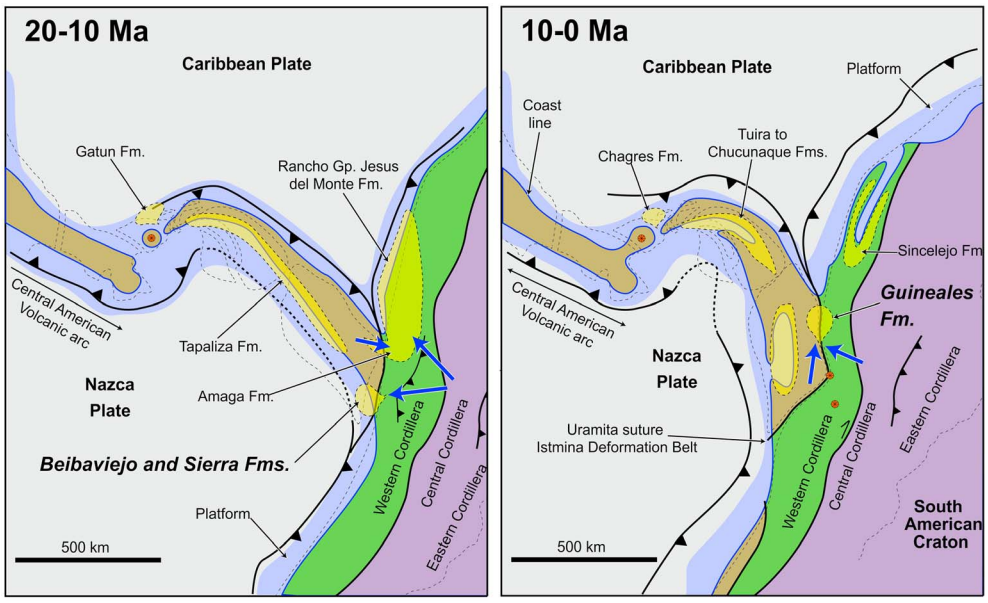

Figure 7. Paleogeographic reconstructions showing possible configurations that would explain the mixed geochronological composition of sediment in the Beibaviejo, Sierra, and Guineales formations. Paleogeographic configuration modified from Montes et al. (2015) and facies distributions from Collins et al. (1996), Coates et al. (2004), Echeverri et al. (2015), and Montes et al. (2010). The blue arrows show suggested sediment paths. The red dots show the proposed active volcanic centers, which are likely to be represented during the 10–0 Ma interval by the El Botón basalt unit (Zapata & Rodríguez, 2011). The shaded colors indicate the different terranes mentioned in the discussion; yellowish brown: Panama Arc, green: CLIP terrain, purple: South American-related continental domain.

postcollisional, late Miocene flat-slab subduction of the Nazca plate underneath South America. They document the construction of a magmatic arc between 14 and 9 Ma on the Western Cordillera, which narrowly postdates and seals the accretion of the Panama Arc. We presented independent evidence that is consistent with the source to sink analysis discussed by Montes et al. (2015) in which a middle Miocene age for the arc-continent collision is proposed. Therefore, the transition from a collisional to a subduction-dominated geodynamic setting took place at ca. 14–12 Ma as suggested by the initiation of continental-arc magmatism.

The results of our inverse thermal modeling show an ongoing pulse of rapid exhumation for the Penderisco Fm during the Pliocene at rates up to 1.0 km/Myr. Furthermore, the integrated exhumation rates of 0.8 to 1.6 km/Myr for the late Miocene-early Pliocene, estimated from the lag-time analysis of the detrital AFT ages of the Sucio River sediments, also suggest that the western flank of the Western Cordillera was being exhumed by that time and the accumulation of the thick conglomeratic sequence of the Guineales Fm. is likely to be the consequence of this period of increased tectonic activity. Geophysical and magmatic constraints suggest the establishment of a late Miocene flat slab that is still active at present north of 5°N (Chiarabba et al., 2015; Syracuse et al., 2016; Wagner et al., 2017). We interpret that deformation and exhumation of the pre-Miocene rocks of the Western Cordillera, as well as the switching from marine-transitional (Beibaviejo Fm.) to high energy terrestrial sedimentary environments during the late Miocene (Guineales Fm.), to represent the upper-plate deformational record of the slab flattening, in which plate coupling may have increased (Finzel et al., 2011; Rosenbaum & Mo, 2011).

6. Conclusions

The Upper Cretaceous-Paleogene Penderisco Fm. nonconformably overlies CLIP fragments accreted to the South American margin and contains the record of such collisional episode.

The Panama Arc in western Colombia includes a Lutetian (~42 Ma) volcano-clastic sequence (Cruces Fm.) composed by interlayered tuffaceous and siliciclastic rocks that contain material derived from basic-intermediate igneous sources with a Panamanian affinity. Continental basement-related related sources are absent.

The provenance of the middle-upper Miocene Sierra Fm. from the Atrato Basin deposited over the Panama Arc basement is characterized by Permo-Triassic and older detrital zircon U-Pb ages. This indicates that docking of the Panama Arc to northwestern South America was complete prior or during the accumulation of this unit. Similarly, the provenance of the middle Miocene Beibaviejo Fm., and the late Miocene-Pliocene Guineales Fm., within the suture zone shows mixed sources from rocks forming both the continental margin and the allochthonous Panama Arc. These detrital signatures further constrain that docking of the Panama Arc to the northwestern corner of South America took place before 12 Ma, as suggested by the intrusive cross-cutting relationship with the El Botón Basalts unit.

Results from the inverse thermal modeling of multiple thermochronometers allow us to identify periods of moderate to rapid exhumation in rocks from the Late Cretaceous to Paleogene Penderisco Fm., as well as for the Buriticá Tonalite. After the onset of cooling/exhumation between the middle Eocene and Oligocene, these units were being moderately rapid exhumed during the middle Miocene, which closely overlaps with the suggested timing for the collision of the Panama Arc and the accumulation of the sediments with mixed provenance from the Atrato Basin and the Western Cordillera. A renewed phase of exhumation is also recorded in upper Miocene-Pliocene strata, which is likely to have been triggered by the flat subduction of the oceanic Nazca plate underneath South America. The Miocene-Pliocene tectonic activity responsible for the late exhumation pulse is also corroborated by the accumulation of the thick conglomeratic sequence of the Guineales Fm., as well as by the integrated exhumation rates obtained from the estimated lag time of the Sucio River sediments (up to 1.6 km/Myr). The above suggests that the orogenic record in western Colombia during the Mio-Pliocene is related to two different tectonic mechanisms: the collision between Panama and South America and the subsequent flat-slab subduction of the Nazca plate.

Acknowledgments

This work was is the result of the MSc. thesis of S. León, and it was supported by the Fundación para la Promoción de la Investigación y la Tecnología (FPIT) (Project 3.809), Asociación Colombiana de Geólogos y Geofísicos del Petróleo (ACGGP), and Corporación Geológica Ares (Project "*Paleogene Accretion-Deformation in Western Colombia: Implications in South-American Continental Growth and Andean Orogeny*"). CAPES provided the MSc. scholarship to S. León. FAPESP provided the young researcher scholarship (2013/03265-5) to M. Parra. The Colombian science foundation COLCIENCIAS supported J.S. Jaramillo, A. Cardona, and G. Monsalve (grants 50491 and 51686). We thank Andréa Jelinek, Claudio Riccomini, and Andrés Bustamante for careful suggestions on the earliest version of this manuscript. J.S. Echeverri, S. Garavito, and S. Betancourt are acknowledged for their help with the organization of heavy mineral data. We are grateful to Laboratório de Espectrometria Gama e Luminescência (Legal) at the University of São Paulo who helped us with the mica etching for AFT analysis. We thank D. Villagómez and an anonymous reviewer for their careful suggestions and comments, which certainly improve the quality of this manuscript. Claudio Faccena is also acknowledged for his helpful comments and the editorial care. Data used in this work can be found in the supporting information.

References

Álvarez, J. (1971). *Informe Preliminar Sobre Geoquímica de la Cordillera Occidental*. Medellín: Ingeominas (Informe Inédito).

Amaya, S., Zuluaga, C. A., & Bernet, M. (2017). New fission-track age constraints on the exhumation of the central Santander Massif: Implications for the tectonic evolution of the Northern Andes, Colombia. *Lithos*, *282–283*, 388–402.

Bacon, C. D., Silvestro, D., Jaramillo, C., Smith, B. T., Chakrabarty, P., & Antonelli, A. (2015). Biological evidence supports an early and complex emergence of the Isthmus of Panama. *Proceedings of the National Academy of Sciences of the United States of America*, *112*(19), 6110–6115. https://doi.org/10.1073/pnas.1423853112

Bartoli, G., Sarnthein, M., Weinelt, M., Erlenkeuser, H., & Lea, D. W. (2005). Final closure of Panama and the onset of northern hemisphere glaciation. *Earth and Planetary Science Letters*, *237*, 33–44. https://doi.org/10.1016/j.epsl.2005.06.020

Bayona, G., Cardona, A., Jaramillo, C., Mora, A., Montes, C., Caballero, V., … Valencia, V. (2013). Onset of fault reactivation in the Eastern Cordillera of Colombia and proximal Llanos Basin; response to Caribbean-South American convergence in early Palaeogene time. In M. Nemčok, A. Mora, & J. W. Cosgrove (Eds.), *Thick-skin-dominated orogens: From initial inversion to full accretion*. *Geological Society of London, Special Publication* (Vol. 377, pp. 285–314).

Bermúdez, M., Hoorn, C., Bernet, M., Carrillo, E., Van der Beek, P. A., Garver, J. I., … Mehrkian, K. (2015). The detrital record of late-Miocene to Pliocene surface uplift and exhumation of the Venezuelan Andes in the Maracaibo and Barinas foreland basins. *Basin Research*, *29*, 370–395. https://doi.org/10.1111/bre.12154

Bourgois, J., Azéma, J., Tournon, J., Bellon, H., Calle, B., Parra, E., … Origlia, I. (1982). Ages et structures des comlplexes basiques et ultrabasiques de la façade pacifique entre 3°N et 12°N (Colombie, Panama et Costa-Rica). *Bulletin De La Société Géologique De Française*, *3*, 545–554.

Brewer, I. D., Burbank, D. W., & Hodges, K. V. (2003). Modelling detrital cooling-age populations: Insights from two Himalayan catchments. *Basin Research*, *15*(3), 305–320. https://doi.org/10.1046/j.1365-2117.2003.00211.x

Buchely, F., Parra, E., Castillo, H., González, F., Dávila, C., & Romero, O. (2009). Realización de la cartografía geológica y muestreo geoquímico en las planchas 144, 145, 128, 129, 113 y 114.

Buchs, D. M., Arculus, R. J., Baumgartner, P. O., Baumgartner-Mora, C., & Ulianov, A. (2010). Late Cretaceous arc development on the SW margin of the Caribbean Plate: Insights from the Golfito, Costa Rica, and Azuero, Panama, complexes. *Geochemistry, Geophysics, Geosystems*, *11*, Q07S24. https://doi.org/10.1029/2009GC002901

Buchs, D. M., Baumgartner, P. O., Baumgartner-Mora, C., Flores, K., & Bandini, A. N. (2011). Upper Cretaceous to Miocene tectonostratigraphy of the Azuero area (Panama) and the discontinuous accretion and subduction erosion along the Middle American margin. *Tectonophysics*, *512*, 31–46. https://doi.org/10.1016/j.tecto.2011.09.010

Burke, K. (1988). Tectonic evolution of the Caribbean. *Annual Review of Earth and Planetary Sciences*, *16*(1), 201–230. https://doi.org/10.1146/annurev.earth.16.1.201

Burton, K. W., Ling, F. H., & O'Nions, R. K. (1997). Closure of the Central American Isthmus and its effect on deep-water formation in the North Atlantic. *Nature*, *386*(6623), 382–385. https://doi.org/10.1038/386382a0

Caballero, V., Mora, A., Quintero, I., Blanco, V., Parra, M., Rojas, L. E., … Duddy, I. R. (2013). Tectonic controls on sedimentation in an intermontane hinterland basin adjacent to inversion structures: The Nuevo Mundo syncline, Middle Magdalena Valley, Colombia. In M. Nemčok, A. Mora, & J. W. Cosgrove (Eds.), *Thick-skin-dominated orogens: From initial inversion to full accretion*, *Geological Society of London, Special Publication* (Vol. 377, pp. 315–342).

Chiarabba, C., De Gori, P., Faccenna, C., Speranza, F., Seccia, D., Dionicio, V., & Prieto, G. A. (2015). Subduction system and flat slab beneath the Eastern Cordillera of Colombia. *Geochemistry, Geophysics, Geosystems*, *17*, 16–27. https://doi.org/10.1002/2014GC005684.Key

Coates, A. G., Collins, L. S., Aubry, M.-P., & Berggren, W. A. (2004). The geology of the Darien, Panama, and the late Miocene-Pliocene collision of the Panama arc with northwestern South America. *Geological Society of America Bulletin*, *116*, 1327–1344. https://doi.org/10.1130/B25275.1

Cochrane, R., Spikings, R. A., Gerdes, A., Ulianov, A., Mora, A., Villagómez, D., … Chiaradia, M. (2014). Permo-Triassic anatexis, continental rifting and the disassembly of western Pangaea. *Lithos*, *190-191*, 383–402. https://doi.org/10.1016/j.lithos.2013.12.020

Collins, L. S., Coates, A. G., Berggren, W. A., Aubry, M.-P., & Zhang, J. (1996). The late Miocene Panama isthmian strait. *Geology*, *24*(8), 687–690. https://doi.org/10.1130/0091-7613(1996)024%3C0687:TLMPIS%3E2.3.CO;2

Coney, P. J., & Evenchick, C. A. (2003). Consolidation of the American Cordilleras. *Journal of South American Earth Sciences*, *7*(3-4), 241–262. https://doi.org/10.1016/0895-9811(94)90011-6

Cooper, M. A., Addison, F., Alvarez, R., Coral, M., Graham, R. H., Hayward, A. B., … Taborda, A. (1995). Basin development and tectonic history of the Llanos Basin, Eastern Cordillera and Middle Magdalena Valley, Colombia. *American Association of Petroleum Geologists Bulletin*, *79*, 1421–1443.

Corfu, F., Hanchar, J. M., Hoskin, P. W. O., & Kinny, P. (2003). Atlas of Zircon Textures. Zircon. *Reviews in Mineralogy and Geochemistry*, *53*, 469–500. https://doi.org/10.2113/0530469

Cortés, M., & Angelier, J. (2005). Current state of stress in the northern Andes as indicated by focal mechanisms of earthquakes. *Tectonophysics*, *403*, 29–58. https://doi.org/10.1016/j.tecto.2005.03.020

Dickinson, W. R. (1985). Interpreting provenance relations from detrital modes of Sandstones. In G. G. Zuffa (Ed.), *Provenance of Arenites* (pp. 333–361).

Dickinson, W. R., Beard, L. S., Brakenridge, G. R., Erjavec, J. L., Ferguson, R. C., Inman, K. F., & Ryberg, P. T. (1983). Provenance of North American Phanerozoic sandstones in relation to tectonic setting. *Geological Society of America Bulletin*, *94*, 222–235. https://doi.org/10.1130/0016-7606(1983)94<222:PONAPS>2.0.CO;2

Dickinson, W. R., & Gehrels, G. E. (2009). Use of U-Pb ages of detrital zircons to infer maximum depositional ages of strata: A test against a Colorado Plateau Mesozoic database. *Earth and Planetary Science Letters*, *288*, 115–125. https://doi.org/10.1016/j.epsl.2009.09.013

Dumitru, T. A. (1991). Effects of subduction parameters on geothermal gradients in forearcs, with an application to Franciscan subduction in California. *Journal of Geophysical Research*, *96*(B1), 621–641. https://doi.org/10.1029/90JB01913

Duque-Caro, H. (1990a). The Choco Block in the northwestern corner of South America: Structural, tectonostratigraphic, and paleogeographic implications. *Journal of South American Earth Sciences*, *3*(1), 71–84. https://doi.org/10.1016/0895-9811(90)90019-W

Duque-Caro, H. (1990b). Neogene stratigraphy, paleoceanography and paleobiogeography in northwest South America and evolution of the Panama Seaway. *Palaeogeography Palaeoclimatology Palaeoecology*, *77*(3-4), 203–234. https://doi.org/10.1016/0031-0182(90)90178-A

Dziewonski, A. M., Chou, T.-A., & Woodhouse, J. H. (1981). Determination of earthquake source parameters from waveform data for studies of global and regional seismicity. *Journal of Geophysical Research*, *86*(B4), 2825–2852. https://doi.org/10.1029/JB086iB04p02825

Echeverri, S., Cardona, A., Pardo-Trujillo, A., Borrero, C., Rosero, S., & López, S. (2015). Correlación y geocronología Ar-Ar del basamento Cretácico y el relleno sedimentario Eoceno Superior-Mioceno (Aquitaniano inferior) de la cuenca de ante-arco de Tumaco, SW de Colombia. *Revista Mexicana de Ciencias Geológicas*, *32*, 179–189.

Ekström, G., Nettles, M., & Dziewonski, A. M. (2012). The global CMT project 2004-2010: Centroid-moment tensors for 13,017 earthquakes. *Physics of the Earth and Planetary Interiors*, *200-201*, 1–9. https://doi.org/10.1016/j.pepi.2012.04.002

Farley, K. A., Wolf, R. A., & Silver, L. T. (1996). The effects of long alpha-stopping distances on (U-Th)/He ages. *Geochimica et Cosmochimica Acta*, *60*(21), 4223–4229. https://doi.org/10.1016/S0016-7037(96)00193-7

Farris, D. W., Jaramillo, C., Bayona, G., Restrepo-Moreno, S. A., Montes, C., Cardona, A., … Valencia, V. A. (2011). Fracturing of the Panamanian Isthmus during initial collision with South America. *Geology*, *39*(11), 1007–1010. https://doi.org/10.1130/G32237.1

Farris, D. W., Cardona, A., Montes, C., Foster, D. A., & Jaramillo, C. (2017). Magmatic evolution of Panama Canal volcanic rocks: A record of arc processes and tectonic change. *PLoS One*, *12*(5), e0176010. https://doi.org/10.1371/journal.pone.0176010

Finzel, E. S., Trop, J. M., Ridgway, K. D., & Enkelmann, E. (2011). Upper plate proxies for flat-slab subduction processes in southern Alaska. *Earth and Planetary Science Letters*, *303*, 348–360. https://doi.org/10.1016/j.epsl.2011.01.014

Fitzgerald, P. G. (2006). Interpretation of (U-Th)/He single grain ages from slowly cooled crustal terranes: A case study from the Transantarctic Mountains of Southern Victoria Land. *Chemical Geology*, *225*, 91–120. https://doi.org/10.1016/j.chemgeo.2005.09.001

Folk, R. L. (1980). *Petrology of sedimentary rocks*. Austin, TX: Hemphill Publishing Company.

Gansser, A. (1973). Facts and theories on the Andes. *Geological Society of London*, *129*(2), 93–131. https://doi.org/10.1144/gsjgs.129.2.0093

Garver, J. I., Brandon, M. T., Roden-Tice, M., & Kamp, P. J. J. (1999). Exhumation history of orogenic highlands determined by detrital fission-track thermochronology. In U. Ring, et al. (Eds.), *Exhumation processes: Normal faulting, ductile flow and erosion*. *Geological Society of London, Special Publication* (Vol. 154, pp. 283–304).

Garzanti, E. (2016). From static to dynamic provenance analysis - Sedimentary petrology upgraded. *Sedimentary Geology*, *336*, 3–13. https://doi.org/10.1016/j.sedgeo.2015.07.010

Gómez, E., Jordan, T. E., Allmendinger, R. W., Hegarty, K., Kelley, S., & Heizler, M. (2003). Controls on architecture of the Late Cretaceous to Cenozoic southern Middle Magdalena Valley Basin, Colombia. *Geological Society of America Bulletin*, *115*, 131–147. https://doi.org/10.1130/0016-7606(2003)115%3C0131:COAOTL%3E2.0.CO;2

Gómez, J., Montes, N. E., Alcárcel, F. A., & Ceballos, J. A. (2015). Catálogo de dataciones radiométricas de Colombia en ArcGIS y Google Earth. In J. Gómez & M. F. Almanza (Eds.), *Compilando La Geología de Colombia: Una Visión a 2015*, *Servicio Geológico Colombiano* (Vol. 33, pp. 63–419). Bogotá: Publicaciones Geológicas Especiales.

Gómez, J., Nivia, A., Montes, N. E., Almanza, M. F., Alcárcel, F. A., & Madrid, C. A. (2015). Notas explicativas: Mapa Geológico de Colombia. In J. Gómez & M. F. Almanza (Eds.), *Compilando La Geología de Colombia: Una Visión a 2015*, *Servicio Geológico Colombiano* (Vol. 33, pp. 9–33). Bogotá: Publicaciones Geológicas Especiales.

González, H. (2001). Mapa Geológico del Departamento de Antioquia. Escala 1:400.000: Memoria Explicativa.

Guenthner, W. R., Reiners, P. W., Ketcham, R. A., Nasdala, L., & Giester, G. (2013). Helium diffusion in natural zircon: Radiation damage, anisotropy, and the interpretation of zircon (U-Th)/He thermochronology. *American Journal of Science*, *313*(3), 145–198. https://doi.org/10.2475/03.2013.01

Haffer, J. (1967). On the geology of the Urabá and northern Chocó regions, northwestern Colombia.

Harley, S. L., Kelly, N. M., & Möller, A. (2007). Zircon behaviour and the thermal histories of mountain chains. *Elements*, *3*, 25–30. https://doi.org/10.2113/gselements.3.1.25

Henry, S. G., & Pollack, H. N. (1988). Terrestrial heat flow above the Andean subduction zone in Bolivia and Peru. *Journal of Geophysical Research*, *93*(B12), 15,153–15,162. https://doi.org/10.1029/JB093iB12p15153

Hincapié-Gómez, S., Cardona, A., Jiménez, G., Monsalve, G., Hoyos-Ramírez, L., & Bayona, G. (2017). Paleomagnetic and gravimetrical reconnaissance of Cretaceous volcanic rocks from the Western Colombian Andes: Paleogeographic connections with the Caribbean Plate. *Studia Geophysica et Geodaetica*. https://doi.org/10.1007/s11200-016-0678-y

Iturralde-Vinent, M. A., & MacPhee, R. D. E. (1999). Paleogeography of the Caribbean region: Implications for Cenozoic biogeography. *Bulletin of the American Museum of Natural History*, *238*, 95.

Jaramillo, C., Montes, C., Cardona, A., Silverstro, D., Antonelli, A., & Bacon, C. D. (2017). Comment (1) on "Formation of the Isthmus of Panama" by O'dea et al. *Science Advances*, *3*, e160231.

Jaramillo, J. S., Cardona, A., León, S., Valencia, V., & Vinasco, C. (2017). Geochemistry and geochronology from Cretaceous magmatic and sedimentary rocks at 6°35′N, western flank of the central cordillera (Colombian Andes): Magmatic record of arc-growth and collision. *Journal of South American Earth Sciences*, *76*, 460–481. https://doi.org/10.1016/j.jsames.2017.04.012

Johnson, J. E., Flowers, R. M., Baird, G. B., & Mahan, K. H. (2017). "Inverted" zircon and apatite (U-Th)/He dates from the Front Range, Colorado: High-damage zircon as a low-temperature (<50°C) thermochronometer. *Earth and Planetary Science Letters*, *466*, 80–90. https://doi.org/10.1016/j.epsl.2017.03.002

Kerr, A. C., Tarney, J., Marriner, G. F., Klaver, G. T. H., & Saunders, A. D. (1996). The geochemistry and tectonic setting of Late Cretaceous Caribbean and Colombian volcanism. *Journal of South American Earth Sciences*, *9*(1-2), 111–120. https://doi.org/10.1016/0895-9811(96)00031-4

Kerr, A. C., Marriner, G. F., Tarney, J., Nivia, A., Saunders, A. D., Thirlwall, M. F., & Sinton, C. W. (1997). Cretaceous basaltic terranes in western Colombia: Elemental, chronological and Sr-Nd isotopic constraints on petrogenesis. *Journal of Petrology*, *38*(6), 677–702. https://doi.org/10.1093/petroj/38.6.677

Ketcham, R. A. (2005). Forward and inverse modeling of low-temperature thermocronometry data. In P. W. Reiners & T. A. Ehlers (Eds.), *Low-Temperature Thermochronology*, *Reviews in mineralogy and Geochemistry* (Vol. 58, pp. 275–314).

Kroonenberg, S. B., Bakker, J. G. M., & van der Wiel, A. M. (1990). Late Cenozoic uplift and paleogeography of the Colombian Andes: Constraints on the development of high-Andean biota. *Geologie en Mijnbouw*, *69*, 279–290.

Leal-Mejía, H. (2011). *Phanerozoic Gold Metallogeny in the Colombian Andes: A Tectono-Magmatic Approach*. Barcelona, Spain: Universidad de Barcelona.

Lonsdale, P. (2005). Creation of the Cocos and Nazca plates by fission of the Farallon plate. *Tectonophysics*, *404*(3-4), 237–264. https://doi.org/10.1016/j.tecto.2005.05.011

Martens, U., Restrepo, J. J., & Solari, L. A. (2012). Sinifaná metasedimentites and relations with Cajamarca paragneisses of the central cordillera of Colombia. *Boletín Ciencias la Tierra*, *32*, 99–109.

Martens, U., Restrepo, J. J., Ordóñez-Carmona, O., & Correa-Martínez, A. M. (2014). The Tahamí and Anacona terranes of the Colombian Andes: Missing links between the South American and Mexican Gondwana margins. *Journal of Geology*, *122*(5), 507–530. https://doi.org/10.1086/677177

Mejía, M., & Salázar, G. (1989). Geología de la plancha 114 (Dabeiba) y parte W de la 115 (Toledo). INGEOMINAS

Montes, C., Guzman, G., Bayona, G., Cardona, A., Valencia, V. A., & Jaramillo, C. (2010). Clockwise rotation of the Santa Marta massif and simultaneous Paleogene to Neogene deformation of the Plato-San Jorge and Cesar-Rancheria basins. *Journal of South American Earth Sciences*, *29*, 832–848. https://doi.org/10.1016/j.jsames.2009.07.010

Montes, C., Cardona, A., McFadden, R., Moron, S. E., Silva, C. A., Restrepo-Moreno, S. A., … Flores, J. A. (2012). Evidence for middle Eocene and younger land emergence in central Panama: Implications for Isthmus closure. *Geological Society of America Bulletin*, *124*(5-6), 780–799. https://doi.org/10.1130/B30528.1

Montes, C., Bayona, G., Cardona, A., Buchs, D. M., Silva, C. A., Morón, S., … Valencia, V. (2012). Arc-continent collision and orocline formation: Closing of the Central American seaway. *Journal of Geophysical Research*, *117*, B04105. https://doi.org/10.1029/2011JB008959

Montes, C., Cardona, A., Jaramillo, C., Pardo, A., Silva, J. C., Valencia, V., … Niño, H. (2015). Middle Miocene closure of the Central American Seaway. *Science*, *348*(6231), 226–229. https://doi.org/10.1126/science.aaa2815

Mora, A., Reyes-Harker, A., Rodriguez, G., Tesón, E., Ramirez-Arias, J. C., Parra, M., … Stockli, D. F. (2013). Inversion tectonics under increasing rates of shortening and sedimentation: Cenozoic example from the Eastern Cordillera of Colombia. In M. Nemčok, A. Mora, & J. W. Cosgrove (Eds.), *Thick-Skin-Dominated Orogens: From Initial Inversion to Full Accretion*, *Special Publication* (Vol. 377, pp. 411–442). London: Geological Society of London. https://doi.org/10.1144/SP377.6

Moreno-Sánchez, M., & Pardo-Trujillo, A. (2003). Stratigraphical and sedimentological constraints on western Colombia: Implications on the evolution of the Caribbean Plate. In C. Bartolini, R. T. Buffler, & J. Blickwede (Eds.), *The circum-gulf of Mexico and the Caribbean: Hydrocarbon habitats, basin formation, and plate tectonics. AAPG Memoir 79*, *Basin Formation, and Plate Tectonics: AAPG Memoir* (pp. 891–924). Tulsa, OK: The American Association of Petroleum Geologists.

O'Dea, A., Lessios, H. A., Coates, A. G., Eytan, R. I., Restrepo-Moreno, S. A., Cione, A. L., … Jackson, J. B. C. (2016). Formation of the Isthmus of Panama. *Science Advances*, *2*(8), e1600883. https://doi.org/10.1126/sciadv.1600883

Pardo-Casas, F., & Molnar, P. (1987). Relative motion of the Nazca (Farallon) and South American Plates since Late Cretaceous time. *Tectonics*, *6*(3), 233–248. https://doi.org/10.1029/TC006i003p00233

Pardo-Trujillo, A., Moreno-Sánchez, M., & Gomez-Cruz, A. D. J. (2002). Estratigrafía de algunos depósitos del Cretáceo Superior en las Cordilleras Central y Occidental de Colombia: Implicaciones Regionales. *Geologie, Ecologie Tropicales*, *26*, 113.

Parra, M., Mora, A., Jaramillo, C., Strecker, M. R., Sobel, E. R., Quiroz, L., … Torres, V. (2009). Orogenic wedge advance in the northern Andes: Evidence from the Oligocene-Miocene sedimentary record of the Medina Basin, Eastern Cordillera, Colombia. *Geological Society of America Bulletin*, *121*(5-6), 780–800. https://doi.org/10.1130/B26257.1

Parra, M., Mora, A., Sobel, E. R., Strecker, M. R., & González, R. (2009). Episodic orogenic front migration in the northern Andes: Constraints from low-temperature thermochronology in the Eastern Cordillera, Colombia. *Tectonics*, *28*, TC4004. https://doi.org/10.1029/2008TC002423

Parra, M., Mora, A., Jaramillo, C., Torres, V., Zeilinger, G., & Strecker, M. R. (2010). Tectonic controls on Cenozoic foreland basin development in the north-eastern Andes, Colombia. *Basin Research*, *22*, 874–903.

Parra, M., Mora, A., López, C., Rojas, L. E., & Horton, B. K. (2012). Detecting earliest shortening and deformation advance in thrust-belt hinterlands: Example from the Colombian Andes. *Geology*, *40*, 171–174.

Pindell, J. L., & Kennan, L. (2009). Tectonic evolution of the Gulf of Mexico, Caribbean and northern South America in the mantle reference frame: An update. In K. H. James, M. A. Lorente & J. L. Pindell (Eds.), *The Geology and Evolution of the Region Between North and South America*, *Special Publication* (pp. 1–60). London: Geological Society.

Ramírez, D. A., Foster, D. A., Min, K., Montes, C., Cardona, A., & Sadove, G. (2016). Exhumation of the Panama basement complex and basins: Implications for the closure of the Central American Seaway. *Geochemistry, Geophysics, Geosystems*, *17*, 1758–1777. https://doi.org/10.1002/2016GC006289

Ramos, V. A. (1999). Plate tectonic setting of the Andean Cordillera. *Episodes*, *22*, 183–190. https://doi.org/10.18814/epiiugs/1999/v22i3/62774

Ramos, V. A., & Folguera, A. (2009). Andean flat-slab subduction through time. In J. B. Murphy, J. D. Keppie, & A. J. Hynes (Eds.), *Ancient Orogens and Modern Analogues*, *Special Publications* (Vol. 327, pp. 31–54). London: Geological Society.

Reiners, P. W., & Brandon, M. T. (2006). Using thermochronology to understand orogenic erosion. *Annual Review of Earth and Planetary Sciences*, *34*(1), 419–466. https://doi.org/10.1146/annurev.earth.34.031405.125202

Restrepo, J. J., Ordóñez-Carmona, O., Armstrong, R., & Pimentel, M. M. (2011). Triassic metamorphism in the northern part of the Tahamí Terrane of the central cordillera of Colombia. *Journal of South American Earth Sciences*, *32*(4), 497–507. https://doi.org/10.1016/j.jsames.2011.04.009

Reyes-Harker, A., Ruiz-Valdivieso, C. F., Mora, A., Ramirez-Arias, J. C., Rodriguez, G., de la Parra, F., … Blanco, V. (2015). Cenozoic paleogeography of the Andean foreland and retroarc hinterland of Colombia. *American Association of Petroleum Geologists Bulletin*, *99*(08), 1407–1453. https://doi.org/10.1306/06181411110

Rodríguez, G., & Arango, M. I. (2013). Formación Barroso: Arco Volcánico Toleítico y Diabasas de San José de Urama: Un Prisma Acrecionario T-MORB en el Segmento Norte de la Cordillera Occidental de Colombia. *Boletín Ciencias la Tierra*, *33*, 17–38.

Rodríguez, G., & Zapata, G. (2012). Características del plutonismo Mioceno Superior en el segmento norte de la Cordillera Occidental e implicaciones tectónicas en el modelo geológico del noroccidente Colombiano. *Bol. Ciencias la Tierra*, *31*, 5–22.

Rodríguez, G., Zapata, G., & Gómez, J. F. (2013). Geología de la plancha 114 - Dabeiba. Escala 1:100.000.

Rodríguez, G., Arango, M. I., Zapata, G., & Bermúdez-Cordero, J. G. (2016). Estratigrafía, Petrografía y Análisis Multi-Método de Procedencia de la Formación Guineales, Norte de la Cordillera Occidental de Colombia. *Boletín Geologie*, *38*(1), 101–124. https://doi.org/10.18273/revbol.v38n1-2016006

Rosenbaum, G., & Mo, W. (2011). Tectonic and magmatic responses to the subduction of high bathymetric relief. *Gondwana Research*, *19*(3), 571–582. https://doi.org/10.1016/j.gr.2010.10.007

Rubatto, D. (2002). Zircon trace element geochemistry: Partitioning with garnet and the link between U-Pb ages and metamorphism. *Chemical Geology*, *184*(1-2), 123–138. https://doi.org/10.1016/S0009-2541(01)00355-2

Ruiz, G. M. H., Seward, D., & Winkler, W. (2004). Detrital thermochronology—A new perspective on hinterland tectonics: An example from the Andean Amazon Basin, Ecuador. *Basin Research*, *16*, 413–430. https://doi.org/10.1111/j.1365-2117.2004.00239.x

Russo, M., & Silver, P. G. (1996). Cordillera formation, mantle dynamics, and the Wilson cycle. *Geology*, *24*(6), 511–514. https://doi.org/10.1130/0091-7613(1996)024%3C0511:CFMDAT%3E2.3.CO;2

Saylor, J. E., Horton, B. K., Stockli, D. F., Mora, A., & Corredor, J. (2012). Structural and thermochronological evidence for Paleogene basement-involved shortening in the axial Eastern Cordillera, Colombia. *Journal of South American Earth Sciences*, *39*, 202–215. https://doi.org/10.1016/j.jsames.2012.04.009

Sinton, C. W., Duncan, R. A., Storey, M., Lewis, J., & Estrada, J. J. (1998). An oceanic flood basalts province within the Caribbean plate. *Earth and Planetary Science Letters*, *155*(3-4), 221–235. https://doi.org/10.1016/S0012-821X(97)00214-8

Somoza, R., & Ghidella, M. E. (2012). Late Cretaceous to recent plate motions in western South America revisited. *Earth and Planetary Science Letters*, *331-332*, 152–163. https://doi.org/10.1016/j.epsl.2012.03.003

Spikings, R. A., & Simpson, G. (2014). Rock uplift and exhumation of continental margins by the collision, accretion, and subduction of buoyant and topographically prominent oceanic crust. *Tectonics*, *33*, 635–655. https://doi.org/10.1002/2013TC003425

Spikings, R. A., Crowhurst, P. V., Winkler, W., & Villagómez, D. (2010). Syn- and post-accretionary cooling history of the Ecuadorian Andes constrained by their in-situ and detrital thermochronometric record. *Journal of South American Earth Sciences*, *30*, 121–133. https://doi.org/10.1016/j.jsames.2010.04.002

Syracuse, E. M., Maceira, M., Prieto, G. A., Zhang, H., & Ammon, C. J. (2016). Multiple plates subducting beneath Colombia, as illuminated by seismicity and velocity from the joint inversion of seismic and gravity data. *Earth and Planetary Science Letters*, *444*, 139–149. https://doi.org/10.1016/j.epsl.2016.03.050

Taboada, A., Rivera, L. A., Fuenzalida, A., Cisternas, A., Philip, H., Bijwaard, H., … Rivera, C. (2000). Geodynamics of the northern Andes: Subductions and intracontinental deformation (Colombia). *Tectonics*, *19*, 787–813. https://doi.org/10.1029/2000TC900004

Toussaint, J. F., & Restrepo, J. J. (1994). The Colombian Andes During Cretaceous Times. In J. A. Salfity (Ed.), *Cretaceous Tectonics of the Andes* (pp. 61–100). Wiesbaden: Vieweg+Teubner Verlag. https://doi.org/10.1007/978-3-322-85472-8_2

Vallejo, C., Spikings, R. A., Luzieux, L., Winkler, W., Chew, D. M., & Page, L. (2006). The early interaction between the Caribbean Plateau and the NW South American Plate. *Terra Nova*, *18*, 264–269. https://doi.org/10.1111/j.1365-3121.2006.00688.x

Vavra, G., Schmidt, R., & Gebauer, D. (1999). Internal morphology, habit and U-Th-Pb microanalysis of amphibolite-to-granulite facies zircons: Geochronology of the Ivrea zone (Southern Alps). *Contributions to Mineralogy and Petrology*, *134*(4), 380–404. https://doi.org/10.1007/s004100050492

Vermeesch, P. (2009). RadialPlotter: A Java application for fission track, luminescence and other radial plots. *Radiation Measurements*, *44*, 409–410. https://doi.org/10.1016/j.radmeas.2009.05.003

Vermeesch, P. (2012). On the visualization of detrital age distributions. *Chemical Geology*, *312–313*, 190–194.

Villagómez, D., & Spikings, R. A. (2013). Thermochronology and tectonics of the Central and Western Cordilleras of Colombia: Early Cretaceous-Tertiary evolution of the Northern Andes. *Lithos*, *160-161*, 228–249. https://doi.org/10.1016/j.lithos.2012.12.008

Villagómez, D., Spikings, R. A., Magna, T., Kammer, A., Winkler, W., & Beltrán, A. (2011). Geochronology, geochemistry and tectonic evolution of the western and central cordilleras of Colombia. *Lithos*, *125*, 875–896. https://doi.org/10.1016/j.lithos.2011.05.003

Vinasco, C., Cordani, U. G., González, H., Weber, M., & Pelaez, C. (2006). Geochronological, isotopic, and geochemical data from Permo-Triassic granitic gneisses and granitoids of the Colombian Central Andes. *Journal of South American Earth Sciences*, *21*, 355–371. https://doi.org/10.1016/j.jsames.2006.07.007

Wagner, L. S., Jaramillo, J. S., Ramírez-Hoyos, L. F., Monsalve, G., Cardona, A., & Becker, T. W. (2017). Transient slab flattening beneath Colombia. *Geophysical Research Letters*, *44*, 6616–6623. https://doi.org/10.1002/2017GL073981

Weber, M., Gómez-Tapias, J., Cardona, A., Duarte, E., Pardo-Trujillo, A., & Valencia, V. (2015). Geochemistry of the Santa Fé batholith and Buriticá Tonalite in NW Colombia—Evidence of subduction initiation beneath the Colombian Caribbean Plateau. *Journal of South American Earth Sciences*, *62*, 257–274. https://doi.org/10.1016/j.jsames.2015.04.002

Wegner, W., Wörner, G., Harmon, R. S., & Jicha, B. R. (2011). Magmatic history and evolution of the Central American land bridge in Panama since Cretaceous times. *Geological Society of America Bulletin*, *123*, 703–724. https://doi.org/10.1130/B30109.1

Zapata, G., & Rodríguez, G. (2011). Basalto de El Botón, Arco Volcánico Mioceno de Afinidad Shoshonítica al Norte de la Cordillera Occidental de Colombia. *Boletín Ciencias la Tierra*, *30*, 77–92.

Zapata, J. P., Cardona, A., Restrepo, J. J., & Martens, U. (2017). Geoquímica y geocronología de las rocas volcánicas básicas y el Gabro de Altamira, Cordillera Occidental (Colombia): Registro de ambientes de Plateau y arco oceánico superpuestos durante el Cretácico. *Boletín Geologie*, *39*(2), 13–30. https://doi.org/10.18273/revbol.v39n2-2017001

Zimmermann, S., & Hall, R. (2016). Provenance of Triassic and Jurassic sandstones in the Banda Arc: Petrography, heavy minerals and zircon geochronology. *Gondwana Research*, *37*, 1–19. https://doi.org/10.1016/j.gr.2016.06.001